2018

3-я Конференция по алгоритмам в Санкт-Петербурге (SPbAW-2018)

(Санкт-Петербург, 28 мая 2018 г.)

Материалы конференции

УДК 004
ББК 22
Т 665

Т 665 3-я Конференция по алгоритмам в Санкт-Петербурге (Санкт-Петербург, 28 мая 2018 г.) Материалы конференции – М.: Мир науки, 2018.– Режим доступа: http://izd-mn.com/PDF/19MNNPK18.pdf — Загл. с экрана.

ISBN 978-5-6041068-8-4

Организатором 3-й конференции по алгоритмам (SPbAW-2018), прошедшей 28 мая 2018 года в Санкт-Петербурге, выступил Российский Научно-исследовательский Центр Технологий Хуавэй (крупный производитель смартфонов в Китае).

Конференция по алгоритмам ИКТ-технологий Хуавэй» - традиционное мероприятие, на котором ведущие российские ученые могут встретиться с действующими коллегами фирмы Huawei Technologies Co. Ltd. и обсудить как открытые исследовательские задачи, так и совместные исследования в области информационных технологий и телекоммуникаций.

В 2018 году конференция был посвящена следующим научным направлениям: линейная и нелинейная обработка сигналов; прием оптимального сигнала; искусственный интеллект для обработки изображений и видео и обработка текстов с использованием естественного языка; информационные технологии, включая разработку программного обеспечения и обработку естественного языка; разработка новых материалов, включая оптические и магнитные материалы.

Публикуемые доклады могут представлять интерес для научных работников, студентов и аспирантов технических вузов.

ISBN 978-5-6041068-8-4

ВЕКТОРНЫЙ ФАЗОВРАЩАТЕЛЬ С НИЗКОЙ ФАЗОВОЙ ОШИБКОЙ НА ОСНОВЕ 0,18 МКМ КМОП-ТЕНХОЛОГИИ И АЛГОРИТМ КАЛИБРОВКИ

Балашов Евгений Владимирович

канд. техн. наук, доцент Института физики, нанотехнологий и телекоммуникаций, Санкт-Петербургский политехнический университет Петра Великого, г. Санкт-Петербург

E-mail: balashov_ev@mail.ru

Коротков Александр Станиславович

докт. техн. наук, профессор, профессор Института физики, нанотехнологий и телекоммуникаций, Санкт-Петербургский политехнический университет Петра Великого, г. Санкт-Петербург

E-mail: korotkov@spbstu.ru

Румянцев Иван Александрович

канд. техн. наук, ассистент Института физики, нанотехнологий и телекоммуникаций, Санкт-Петербургский политехнический университет Петра Великого, г. Санкт-Петербург

E-mail: i.a.rumiantsev@spbstu.ru

VECTOR-SUM PHASE SHIFTER WITH LOW PHASE ERROR IN 0.18 UM CMOS AND ITS CALIBRATION ALGORITHM

Evgenii Balashov

Ph. D. in Technical Sciences, Associate Professor of Institute of Physics, Nanotechnology and Telecommunications, Peter the Great St.Petersburg Polytechnic University, Saint Petersburg

Alexander Korotkov

Doctor of Technical Science, Professor, Professor of Institute of Physics, Nanotechnology and Telecommunications, Peter the Great St.Petersburg Polytechnic University, Saint Petersburg

Ivan Rumyancev

Ph. D. in Technical Sciences, Assistant Professor of Institute of Physics, Nanotechnology and Telecommunications, Peter the Great St.Petersburg Polytechnic University, Saint Petersburg

АННОТАЦИЯ

В работе представлен интегральный шестиразрядный векторный фазовращатель, разработанный по 0,18 мкм КМОП-технологии. Максимальная и среднеквадратичная фазовые ошибки в диапазоне рабочих частот 2,8-3,2 ГГц не превышают 1,5 и 0,9 градуса соответственно. Для минимизации влияния разброса параметров технологического процесса разработан и реализован алгоритм определения управляющих напряжений на основе интерполирования измеренных зависимостей модуля и фазы коэффициента передачи от управляющих напряжений.

ABSTRACT

The paper presents an unbalanced transformerless 6-bit vector-sum phase shifter in a standard 0.18 μm CMOS technology. Maximum and RMS phase errors in 2.8-3.2 GHz band are below 1.5 and 0.9 degree respectively. Calibration algorithm for determining the control voltages is developed and implemented based on interpolation of the measured dependences of the magnitude and phase of the transmission coefficient on the control voltages to minimize the influence of the technological parameters variation.

Ключевые слова: векторный фазовращатель; калибровка; КМОП-технология.

Keywords: vector-sum phase shifter; calibration; CMOS technology.

INTRODUCTION

Active phase arrays are widely used in radar and communication. A typical array of this kind comprises up to several thousand transceivers built according to the simplified block diagram shown in Fig. 1. The transmitting path consists of an attenuator (ATT), a phase shifter (PHS) and a power amplifier (PA). The receiving path consists of a low-noise amplifier (LNA), a phase shifter and an attenuator. Circulators or RF switches (SW) separate the receiving and transmitting paths. So, a phase shifter is a core element of a transceiver and is used to change the phase of the input RF signal according to the external digital control signal.

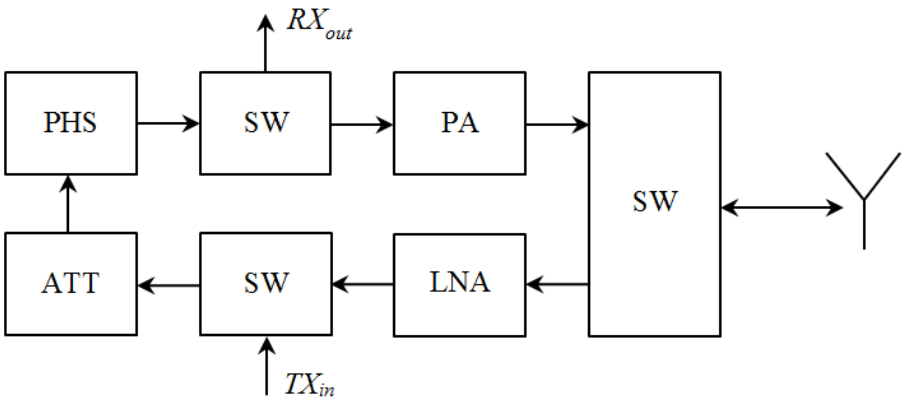

Fig. 1. Block diagram of a transceiver

There are different types of phase shifters [1], such as vector-sum, reflective, transmission line based and switched, the latter being the most popular commercial solution. However, such phase shifters feature high losses and phase errors due to technological parameters variation while the phase error is the key characteristic.

Vector-sum phase shifters have been the subject of close attention in recent years [2]-[4] because of their ability to be post-calibrated thus reducing the effect from uncontrolled scatter in technological parameters. Vector diagrams in Fig. 2 illustrate vector-sum phase shifter principle of operation. The unbalanced input signal is transformed into a balanced one to form orthogonal components. A pair of the orthogonal components is then selected according to the digital control signal to be

further weighted by variable gain amplifiers to be summed into a phase shifted output signal.

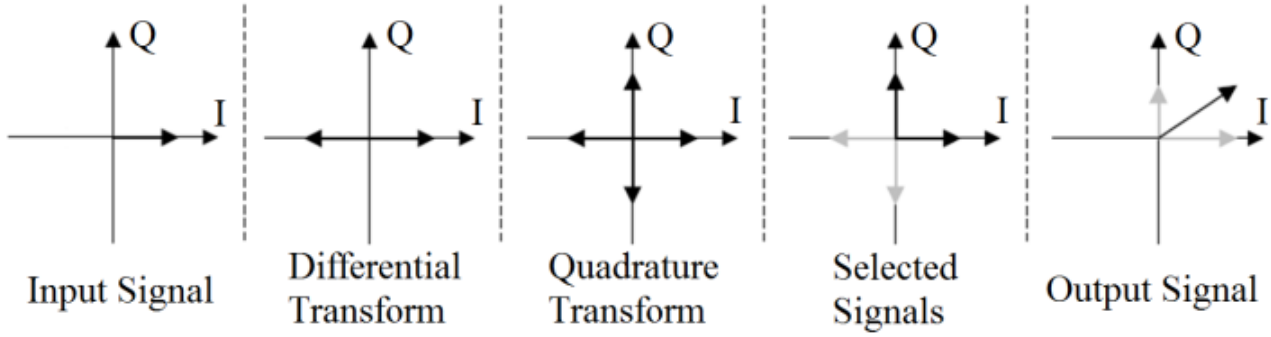

Fig. 2. Vector diagrams

Traditionally, phase shifters are implemented using III-V technologies such as GaAs. However, keeping in mind how big the number is of transceivers in an array, silicon-based technology seems promising as for production cost and integration level of a chip. The paper describes an unbalanced transformerless 6-bit vector-sum phase shifter implemented in a standard 0.18 μm CMOS technology and its post-silicon calibration algorithm.

PROPOUSED PHASE SHIFTER ARCHITECTURE

The block diagram of the RF part of the designed vector-sum phase shifter is shown in Fig. 3. It includes: an all-pass RC-filter (QAF), two variable gain amplifiers (VGA), a common-mode rejection circuit (CMRC), an active balun (Balun) and an output amplifier (AMP).

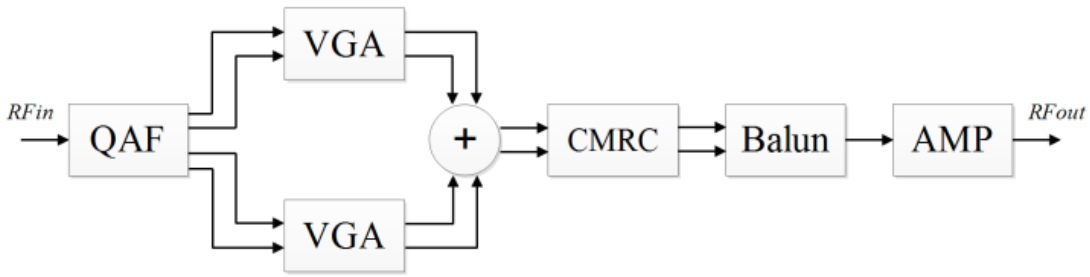

Fig. 3. Block diagram of the RF unit

Since the phase error is increased due to amplitude and phase errors during multiple signal transforms along the RF path, those transforms should be reduced as much as possible. To this end, the all-pass RC-filter with unbalanced input is proposed to form quadrature signals directly out of the unbalanced one skipping the balanced-unbalanced signal transform. The RC-filter with input matching inductor is shown in Fig. 4a. Since the variable gain amplifiers do not suppress enough the common-mode component, additional suppression was implemented using the circuit in Fig. 4b.

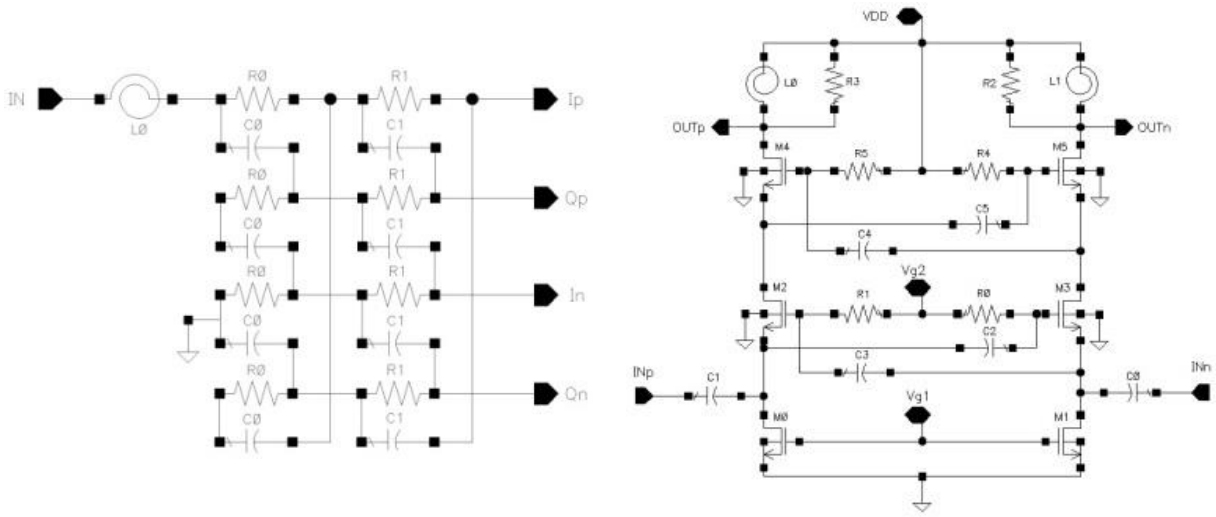

(a) (b)

Fig. 4. (a) RC-filter and (b) common-mode rejection circuit

CALIBRATION ALGORITHM

Several calibration algorithms are presented in papers. A calibration algorithm based on calculation of control voltages in accordance with information about the magnitude and phase of the transmission coefficient for different values of the control voltage is proposed in [5]. However, due to leakage of quadrature signals, the calculated values may differ significantly from the optimal ones. Authors reports the amplitude and phase errors at the central frequency are 0.8 dB and 7 degrees respectively.

Another algorithm is used in [6]. Firstly, the magnitude and phase of the transmission coefficient are measured for all possible states, and then only states that meet the specified requirements are selected. The disadvantage of this approach is a significant increase in the time required to calibrate a single sample. Depending on the number of states it could take up to several hours.

In this paper, an algorithm that eliminates the problems of the approaches discussed above is proposed:

1) required values of amplitude (*MagErr*) and phase (*PhErr*) errors, control voltages step (*dU)* are set;

2) dependences of the magnitude and phase of the transmission coefficient $S_{21_{i,j}}$ on control voltages U_i and U_j with *dU* are measured;

3) two-dimensional interpolation of the resulting matrix is performed;

4) the magnitude $\left(|S_{21_{max,0}}|\right)$ and phase $\left(arg\left(S_{21_{max,0}}\right)\right)$ of the transmission coefficient in zero state is determined;

5) truncation of the interpolated matrix by the criterion $||S_{21_{i,j}}|-|S_{21_{max,0}}|| \leq MagErr$ is performed;

6) the phase state and corresponding pair of control voltages are searched by the criterion $arg\left(S_{21_{i,j}}\right) - arg\left(S_{21_{max,0}}\right) \leq PhErr$.

MEASUREMENT RESULTS

Fig. 5 shows the die micrograph of the fabricated 6-bit phase shifter. The die area is 5.3 sq. mm, the core area is of 3.3 sq. mm. The circuit consumes 55 mA from 1.8 V supply.

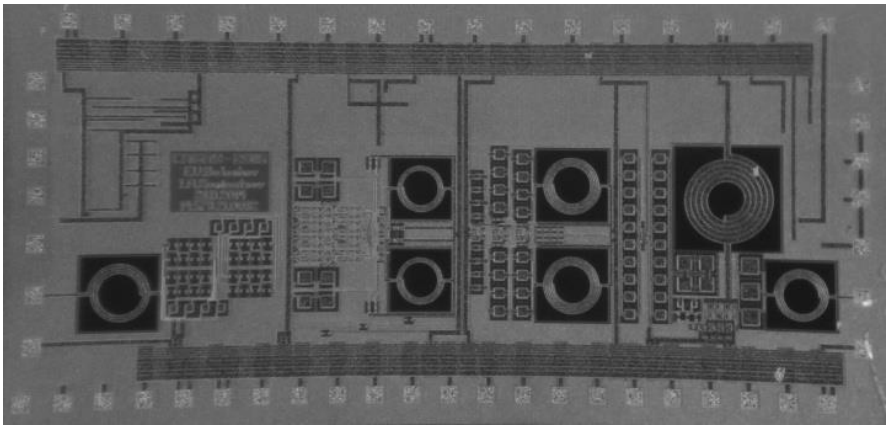

Fig. 5. Die micrograph

The Rohde & Schwarz ZVA40 vector network analyzer, Arduino Mega board and MAX5533 DACs were used to measure the scattering matrix parameters. Calibration and measurements were automated and post-processed using the designed LabVIEW program.

Fig. 6a shows gain magnitude versus frequency for 64 phase states the lowest value within 2.8-3.2 GHz being of 1.7 dB. The maximum gain error stays below 0.45 dB at switching between the phase states as Fig. 6b indicates.

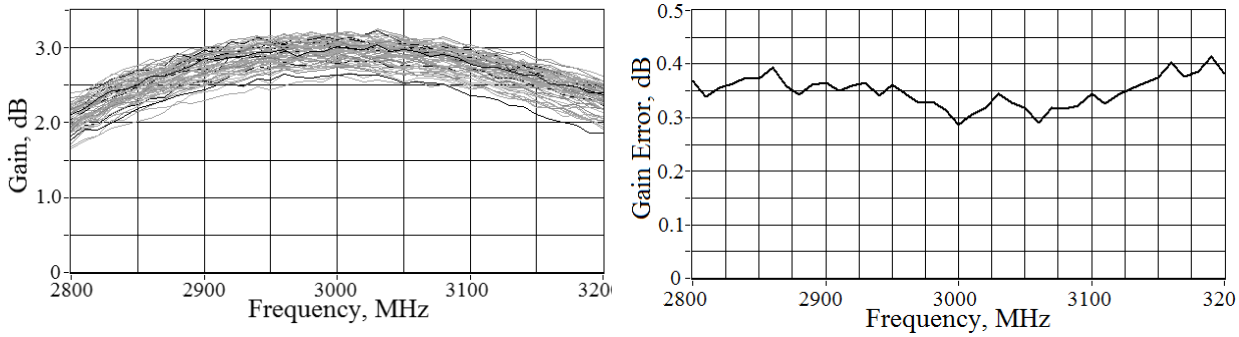

(a) (b)

Fig. 6. (a) Gain magnitude and (b) gain error

In Fig. 7a the gain phase is plotted against frequency for all the phase states. Then absolute and RMS errors were calculated out of these data. The RMS error versus frequency is depicted in Fig 7b and stays below 0.9 degree.

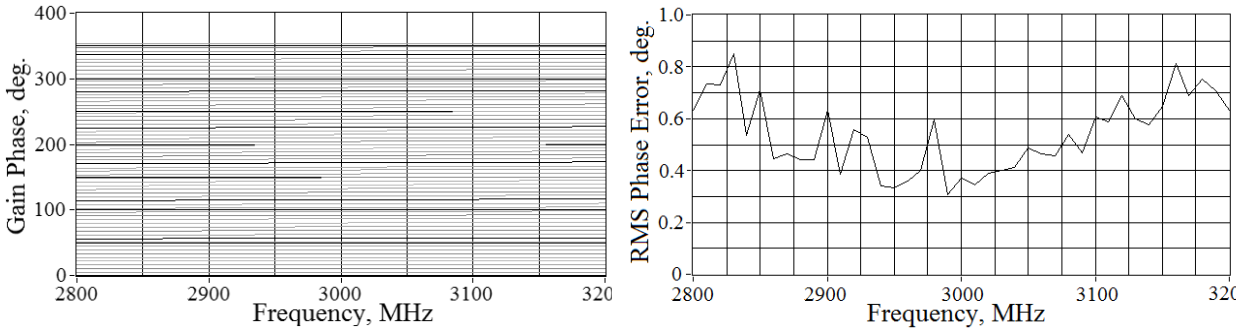

(a) (b)

Fig. 7. (a) Relative phase and (b) RMS phase error

CONCLUSION

The paper presents an unbalanced transformerless 6-bit vector-sum phase shifter in a standard 0.18 μm CMOS with maximum phase error of 1.5 deg. and RMS phase error below 0.9 deg. in 2.8-3.2 GHz band. Table 1 gives a summary about how the designed phase shifter compares to its analogs. Use of the proposed calibration algorithm allowed the reduce of calibration time up to 20 times compared to the algorithm based on measurement of all states.

Table 1.

Phase shifters' characteristics in comparison

	[2]	**[3]**	**[7]**	**[8]**	**[9]**	**This work**
Type	Vector	Vector	Switched	Switched	Switched	Vector
Frequency, GHz	2.3-3.7	4.0-6.0	2.5-3.2	2.5-3.1	3.4-4.0	2.8-3.2
Gain, dB	–4.5	4.0	–4.5	–6.5	–5	1.7
Gain error, dB	0.65*	0.3*	1.5	0.4	1.5	0.45
RMS phase error, deg.	1.4	1.2	2.0	2.0	-	0.9
Power, mW	19	51	60	53	38	99
Technology	0.18 µm CMOS	0.25 µm SiGe	0.18 µm CMOS	GaAs	0.5 µm GaAs	0.18 µm CMOS

*RMS

REFERENCES

[1] F. Ellinger, et al., "Integrated Adjustable Phase Shifters," IEEE Microwave Magazine, vol. 11, no. 6, Oct. 2010, pp. 97-108.

[2] A. Asoodeh, M. Atarodi, "A Full 360 Vector-Sum Phase Shifter With Very Low RMS Phase Error Over a Wide Bandwidth," IEEE Trans. on Microwave Theory and Techniques, vol. 60, no 6, June 2012, pp. 1626–1634.

[3] I. V. Malishev, I. I. Mukhin, V. V. Repin, A. S. Shnitnikov, "Development of a phase shifter LSI for radar applications," Int. Crimean Conference "Microwave & Telecommunication Technology", Sevastopol, 2011, pp. 149-150.

[4] E. V. Balashov, I. A. Rumyancev, "A fully integrated 6-bit vector-sum phase shifter in 0.18 um CMOS," International Siberian Conference on Control and Communications, Omsk, 2015, pp. 1-5.

[5] F. Ellinger, U. Lott, W. Bachtold, "An antenna diversity MMIC vector modulator for HIPERLAN with low power consumption and calibration capability", Trans. on Microwave Theory and Techniques, vol. 49, no. 5, May 2001, pp. 964-969.

[6] K.M. Amburkin, G.V. Chugukov, Metodika optimizacii tochnostnyh parametrov vektornyh SVCH fazovrashchatelej, Tverdotel'naya ehlektronika.

Slozhnye funkcional'nye bloki REHA, materialy nauchno-tekhnicheskoj konferencii, M.: MNTOREHS im. A.S.Popova, 2011, P. 46-48. (in Russian)

[7] M. Meghdadi, M. Azizi, M. Kiani, A. Medi, M. Atarodi, “A 6-Bit CMOS Phase Shifter for S-Band,” IEEE Trans. on Microwave Theory and Techniques, vol. 58, no. 12, Dec. 2010, pp. 3519-3526.

[8] HMC647 technical documentation. Available at (accessed 20.04.2018): http://www.analog.com/media/en/technical-documentation/data-sheets/hmc647.pdf

[9] MP308 technical documentation. Available at (accessed 20.04.2018): http://www.micran.ru/productions/MIS/shifters/MP308/.

ИСПОЛЬЗОВАНИЕ КОНЕЧНО-СХОДЯЩИХСЯ АЛГОРИТМОВ ДЛЯ ФУНКЦИОНАЛЬНОЙ ИДЕНТИФИКАЦИИ

Бондарко Владимир Александрович

канд. физ.-мат. наук, доцент кафедры теоретической кибернетики математико-механического факультета Санкт-Петербургского университета, г. Санкт-Петербург

E-mail: vbondarko@gmail.com

USING OF FINITELY-CONVERGENT ALGORITHMS FOR FUNCTIONAL IDENTIFICATION

Vladimir Bondarko

candidate of Science, associate professor of Theoretical Cybernetics department, faculty of mathematics and mechanics, St. Petersburg University, St. Petersburg

АННОТАЦИЯ

Конечно-сходящиеся алгоритмы первоначально разрабатывались для настройки весов персептрона Розенблатта, а затем успешно применялись в качестве алгоритмов адаптации в рамках предложенного В.А.Якубовичем метода рекуррентных целевых неравенств. Они не требуют стохастических свойств от внешних воздействий на идентифицируемую систему. Состоятельность оценок не гарантирована, но в некотором смысле они не хуже, чем истинные значения оцениваемых параметров. Реализация алгоритмов не требует значительных вычислительных ресурсов.

ABSTRACT

Finitely-convergent algorithms were originally developed to tune the Rosenblatt's perceptron. Later on, they were tailored for adaptive control of dynamical systems within the framework of the general approach proposed by V.A. Yakubovich under

the name of the ``method of recurrent targeted inequalities". Unlike many competing approaches, these algorithms do not rely on certain stochastic properties of external disturbances on the identified system. Though the consistency of the resultant estimates is not guaranteed in general, it can be shown that they are not worse than the true values of the assessed parameters from a certain point of view. An extra benefit is that implementation of these algorithms does not call for considerable computational resources.

Ключевые слова: онлайн идентификация; конечно-сходящиеся алгоритмы.

Keywords: online identification, finitely-convergent algorithms.

1. From perceptron to identification/adaptation algorithms: "YaVA" and "Stripe".

Historically, finitely-convergent algorithms stem from the problem of perceptron tuning. Namely, let the training sequence consist of two vector sets

$$X_1 = \{x_i\}_{i=1}^{n}, X_2 = \{x_j\}_{j=n+1}^{N}.$$

The problem is to find parameters α, θ of a hyperplane $H = \{x: \alpha + (\theta, x) = 0\}$ such that H separates X_1 and X_2:

$$\alpha + (\theta, x) < 0 \ \forall x \in X_1, \alpha + (\theta, x) > 0 \ \forall x \in X_2, \quad (1)$$

where $(\cdot,\cdot)$stands for the dot. This problem should be solvable, i.e. there should exist $\bar{\alpha}, \bar{\theta}$ such that inequalities (1) satisfied for $\alpha = \bar{\alpha}, \theta = \bar{\theta}$. Without any loss of generality we obviously may assume that

$$\bar{\alpha} + (\bar{\theta}, x) < -\varepsilon \ \forall x \in X_1, \bar{\alpha} + (\bar{\theta}, x) > \varepsilon \ \forall x \in X_2 \quad (2)$$

for arbitrary predefined $\varepsilon > 0$.

The dual problem is to find a point (vector) $\tau = \begin{bmatrix} \alpha \\ \theta \end{bmatrix}$ which lies in different sides of hyperplanes $(\tau, \phi_i) = 0$ in dependency on which x_i comprises of $\phi_i = \begin{bmatrix} 1 \\ x_i \end{bmatrix}$. More convenient is to define $\varphi_i = \begin{bmatrix} 1 \\ x_i \end{bmatrix}$ for $x_i \in X_1$ and $\varphi_i = \begin{bmatrix} -1 \\ -x_i \end{bmatrix}$ for $x_i \in X_2$. Thus we find τ such that $(\tau, \varphi_i) < 0$ or $\varepsilon + (\tau, \varphi_i) \leq 0 \; \forall i$.

So the problem of perceptron weights adjusting reduces to the system of inequalities of the sort

$$\alpha_k - (\tau, \varphi_k) < 0 \, , k = 0,1, \dots \, , \tag{3}$$

where φ_k is repeated in a circular manner. In [3] V.A.Yakobovich proposed an algorithm

$$\tau_k = \begin{cases} \tau_{k-1}, & \text{if } \alpha_k - (\tau_{k-1}, \varphi_k) \leq 0, \\ \tau_{k-1} + \frac{\alpha_k - (\tau_{k-1}, \varphi_k) + \varepsilon}{|\varphi_k|^2} \, \varphi_k, & \text{if } \alpha_k - (\tau_{k-1}, \varphi_k) > 0, \end{cases} \tag{4}$$

$$k = 0,1, \dots \, ,$$

which was named as “YaVA” in his honor. This algorithm converges after finite many steps, if there exists a τ such that $\alpha_k - (\tau, \varphi_k) < -\varepsilon \; \forall k$.

Let us now consider a discrete-time linear time-invariant dynamic system

$$y_k + a_1 \, y_{k-1} + \dots + a_n \, y_{k-n} = b_1 \, u_{k-1} + \dots + b_n \, u_{k-n} + v_k, \tag{5}$$

where $k = 0,1, \dots$, coefficients a_j, b_j are unknown, input $\{u_k\}$ and output $\{y_k\}$ are observable signals, and $\{v_k\}$ is a uniformly bounded unobservable noise:

$$|v_k| \leq C \; \forall k. \tag{6}$$

Suppose that coefficients $\hat{a}_j, \hat{b}_j$ are found such that

$$\hat{v}_k = y_k + \hat{a}_1 \, y_{k-1} + \dots + \hat{a}_n \, y_{k-n} - \hat{b}_1 \, u_{k-1} - \; \dots - \hat{b}_n \, u_{k-n}$$

satisfy inequalities

$$|\hat{v}_k| \le \hat{C}\ \forall k. \tag{7}$$

Then the equation

$$y_k + \hat{a}_1\, y_{k-1} + \ldots + \hat{a}_n\, y_{k-n} = \hat{b}_1\, u_{k-1} + \ \ldots + \hat{b}_n\, u_{k-n} + \hat{v}_k$$

describes the system at hands as well as (5), even if $\hat{a}_j \neq a_j$ and $b_j \neq \hat{b}_j$ for any or all j. From this point of view $\hat{a}_j, \hat{b}_j$ are the estimates of the coefficients a_j, b_j in (5). A quality of these estimates depends on relation between the constants C and $\hat{C}$ in inequalities (6) and (7). The basic question is how these estimates should be obtained. Let us define $\tau = \begin{bmatrix} b_1 \\ \vdots \\ b_n \\ -a_1 \\ \vdots \\ -a_n \end{bmatrix}, \varphi_k = \begin{bmatrix} u_k \\ \vdots \\ u_{k-n+1} \\ y_k \\ \vdots \\ y_{k-n+1} \end{bmatrix}$. Then inequalities (7) may be rewritten as

$$|y_k - (\tau, \varphi_{k-1})| \le \hat{C}\ , k = 0,1, \ldots\ ., \tag{8}$$

Every of them is equivalent to a pair of inequalities resembling (3): $-y_k + (\tau, \varphi_{k-1}) \le \hat{C}$ and $y_k - (\tau, \varphi_{k-1}) \le \hat{C}$. Applying the algorithm YaVA to both of these inequalities yields the following

$$\tau_k = \begin{cases} \tau_{k-1}, & \text{if } |\eta_k| \le \hat{C}, \\ \tau_{k-1} + \ \mu_k \eta_k \dfrac{1 - \rho\hat{C}/|\eta_k|}{|\varphi_{k-1}|^2}\ \varphi_{k-1}, & \text{if } |\eta_k| > \hat{C}, \end{cases} \qquad k = 0,1, \ldots\ , \tag{9}$$

where $\eta_k = y_k - (\tau, \varphi_{k-1})$, μ_k and ρ are auxiliary parameters. They should satisfy inequalities $1/2 \le \mu_k \le 1$, $\rho\hat{C} \le C$, $0 < \rho < 1$. The algorithm (9) is known under the name “Stripe” since each inequality (8) selects a gap between two parallel hyperplanes $y_k - (\tau, \varphi_{k-1}) = \pm\hat{C}$ in a vector space of τ.

Benefits from applying the "Stripe" algorithm to identification task may be demonstrated by means of an example concerned with adaptive suboptimal control of the minimal-phase system (5) with uniformly bounded disturbance (6). Equation $(\tau, \varphi_k) = 0$ describes optimal controller minimizing $J \stackrel{\text{def}}{=} \sup\limits_{\{v_k\}:(6)} \operatorname{limsup}\limits_{k\to\infty} |y_k|$. Since we don't know τ, we use the controller

$$(\tau_k, \varphi_k) = 0 \qquad (10)$$

instead, where τ_k are developed by the algorithm (9). These controller guaranties the inequality $|y_k| = |y_k - (\tau_k, \varphi_k)| \le \hat{C}$ for all sufficiently large k, though $\lim\limits_k \tau_k$ may differ from the true value of τ. Nevertheless, $\hat{C}$ may be chosen as close to C as desired, where $C = \inf J$. In this sense "Stripe" guaranties **functional** identification of the system (5).

Typical simulation results are presented in figures 1,2. The system (5) has minimal dimension: $y_k - 1.3y_{k-1} = 1.75u_{k-1} + v_k$, disturbance v_k is uniformly distributed over [-1,1]. Thus true value of vector τ is $\begin{bmatrix}1.75\\1.3\end{bmatrix}$. Starting point τ_0 is equal to $\begin{bmatrix}0.1\\-1\end{bmatrix}$, final point $\lim\limits_k \tau_k = \tau_4 \approx \begin{bmatrix}2.28\\1.62\end{bmatrix} \ne \tau$, but figure 2 demonstrates high performance of adaptive control: $|y_k| < 1$ for all $k > 4$,

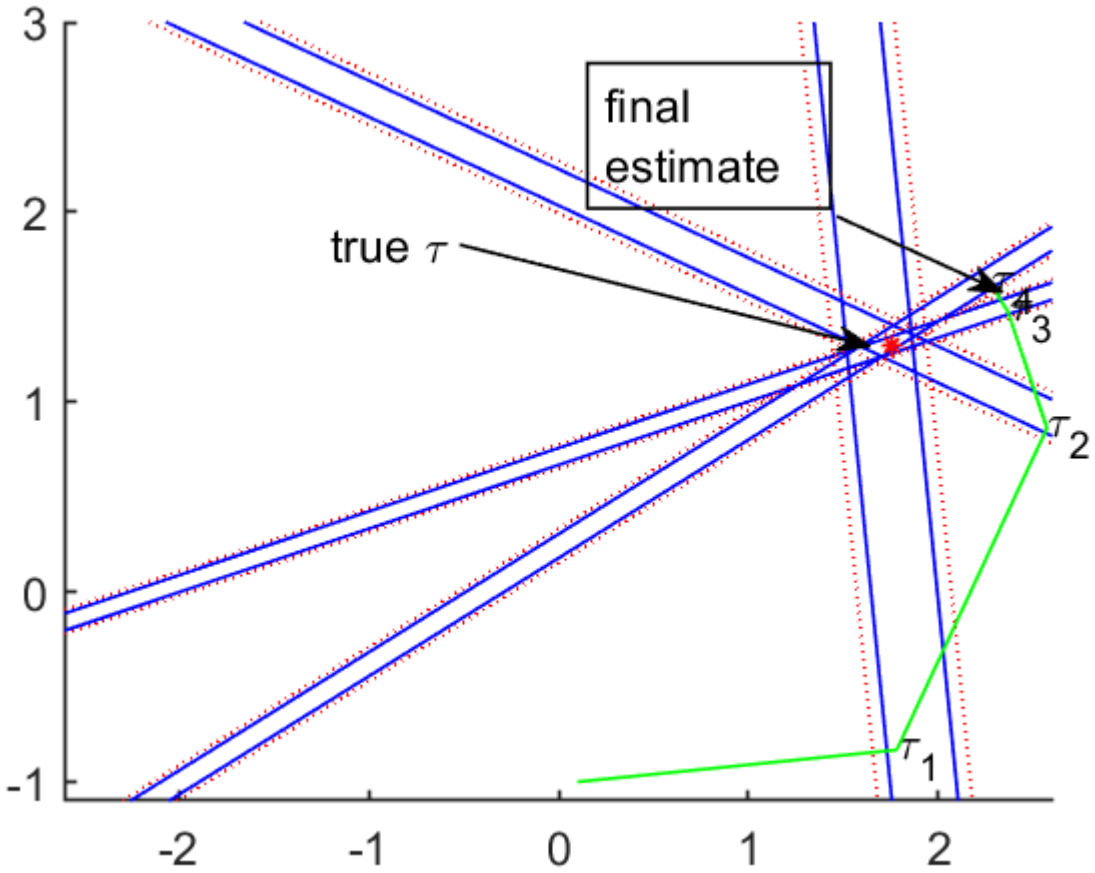

Fig. 1. Trajectory of estimates.

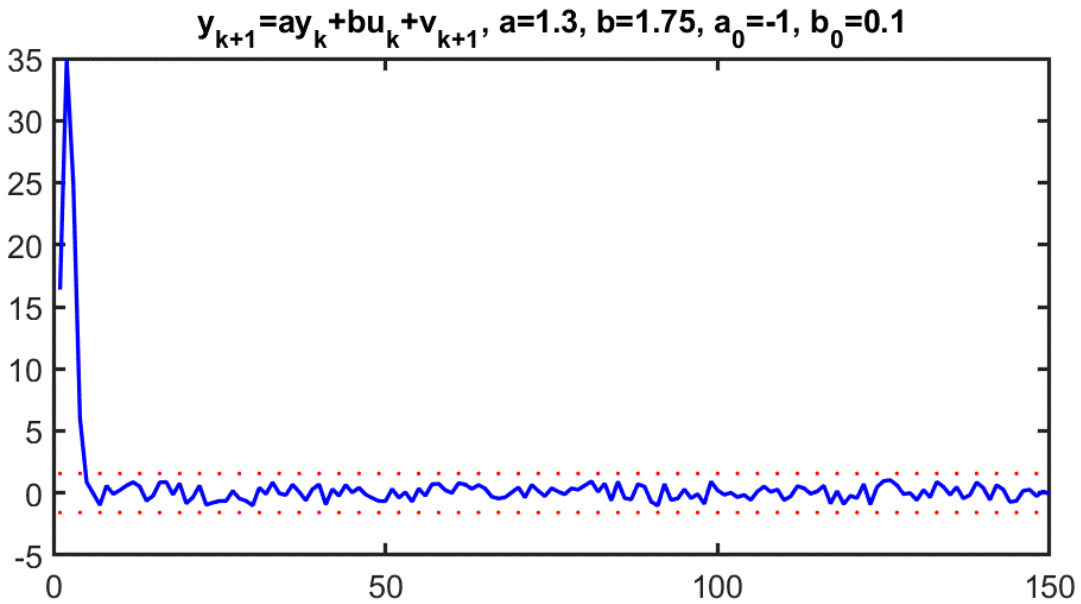

Fig. 2. System output; dotted lines mark optimal level of output.

2. Development of finite-convergent algorithms.

Algorithm “Stripe” is convenient due to its simplicity and insensitivity to stochastic characteristics of the signals involved: it does not matter how the noise is distributed, only its boundedness is of value. Hence these signals may nonlinearly depend on other signals (possibly with known probability distributions), which does not undermine the high performance of the algorithm. Instead of uniformly bounded noise, one may consider [2] the inequalities of the following form

$$\sum_{j=0}^{N}\left|y_{k-j}-\left(\tau,\varphi_{k-j-1}\right)\right|^2 \le C\ , \tag{11}$$

or

$$\limsup_{k\to\infty}\frac{1}{k}\sum_{j=0}^{k}\left|y_j-\left(\tau,\varphi_{j-1}\right)\right|^2 \le C\ . \tag{12}$$

Finitely-convergent algorithms are developed for both cases, see [2]. Inequalities (11) are, for example, very natural in relation with the problem of noisy channel equalization, because in this case all digital processing performs frame by frame of the length N using fast Fourer transform. Inequalities (12) allow us to consider any stochastic noise with the variance $\sigma^2 < C$ independently of its distribution.

Another direction is considering [1] inequalities of the sort

$$\left|y_k-(\tau,\varphi_{k-1})-(f(\tau),\phi_{k-1})\right| \le \hat{C}\ , k=0,1,\dots\ , \tag{13}$$

where $f(\tau)$ is nonlinear function, ϕ_k is observable signal. Though these inequalities may describe nonconvex areas in vector space of τ, finitely-convergent algorithms developed for this case, too. For example, the problem of field-oriented control of induction motor is mixed up with the inequalities

$$\left|\left|\tau-c_k\right|^2-r_k^2\right| \le \varepsilon\ , k=0,1,\dots \tag{13}$$

on 2-vectors τ. These inequalities mark a sequence of rings with centers c_k. Finetely-convergent algorithm successfully finds a point in intersection of all these rings:

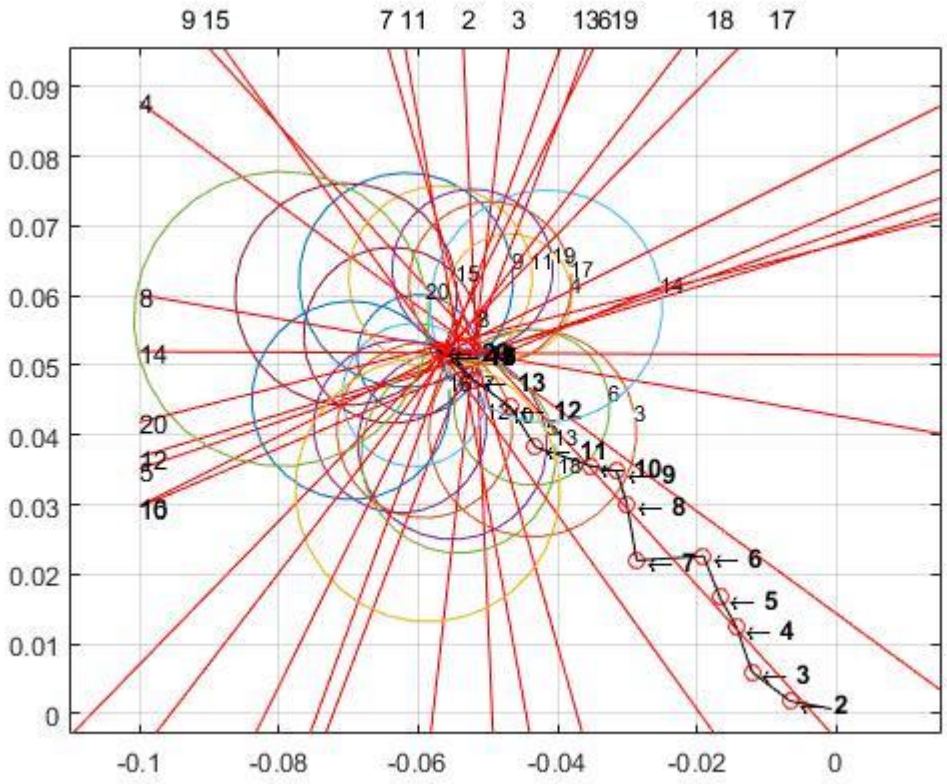

Fig 3. Solving of nonconvex inequalities by finitely-convergent algorithm. Trajectory of estimates.

Conclusion.

The paper presents an evidence that finitely-convergent algorithms form an effective approach to many problems in the areas of identification and control.

Список литературы.

1. Бондарко В.А. Адаптивное векторное управление асинхронным электродвигателем на основе метода рекуррентных целевых неравенств //Автоматика и телемеханика. —2010. —№ 9. С. 120-135.

2. Гусев С.В. Конечно-сходящийся алгоритм восстановления функции регрессии и его применение в задачах адаптивного управления // Автоматика и телемеханика. – 1989. – №3. – С. 99–108
3. Якубович В.А. Рекуррентные конечно сходящиеся алгорифмы решения систем неравенств // ДАН СССР. —1966. —Т.166. —N6. С.1308--1312.

ИНВАРИАНТНАЯ ЛОКАЛИЗАЦИИЯ ГРАФИЧЕСКИХ ОБЪЕКТОВ ПЛОСКОЙ СЦЕНЫ

А. Ю. Дорогов

Д.т.н., доцент, Санкт-Петербургский государственный электротехнический университет «ЛЭТИ», Россия, Санкт-Петербург

e-mail: vaksa2006@yandex.ru

INVARIANT LOCALIZATION OF GRAPHIC OBJECTS IN FLAT SCENES

A.Yu. Dorogov

Doctor of science, docent, Saint Petersburg state electrotechnical university "LETI", Russia, Saint Petersburg

e-mail: vaksa2006@yandex.ru

АННОТАЦИЯ

Предложенный метод локализации графических объектов плоской сцены является инвариантным к условиям освещения, смещению масштабированию и повороту объектов. Метод основан на векторном представлении образов сцены и искомого объекта. В работе представлена модель построения паттерна объекта. Показаны результаты использования метода для реальных изображений.

ABSTRACT

The proposed localization method for graphical objects of scene image is invariant to the illuminance conditions, scale, offset and rotation of the objects. The method is based on a vector representation of scene image and searched object. Model for building of object pattern and algorithm of its recognition are represented. Experimental results for real images are shown.

Ключевые слова: инвариант; графический объект; распознавание; локализация.

Keywords: Invariant; graphical object; scene image; recognition; localization.

Introduction

A significant amount of aerospace data is presented by means images of the earth's surface in the form of flat scenes with a set of objects of interest.

Currently, the rate of receipt of earth observation data has increased significantly, therefore the problem of automation of processes of scene analysis is actual. The key technological challenge is the detection of known objects in an unknown scene. A feature of the analysis process aerospace images is a wide variation in characteristics, in lighting conditions, in location and size of the objects in image diversity. Therefore, the detection algorithms should possess the properties of invariance to the above listed characteristics.

In this paper, we propose a method of locating graphics objects bitmap images with invariance to lighting conditions, displacement, rotation and scaling of the object images on a flat stage. Object in a scene is localized by the coordinates of the center of the rectangular fragment that contains the object and the size of the fragment in the current scene. The algorithm is based on the use of vector descriptions of scene and contour of the image of the desired object. Thanks to the vectoring, it is provided invariance of the search algorithm relatively to the light conditions of the object and the robustness to possible distortions of the source bitmap. Algorithms of vectorization are fairly well developed [1] and in this article are not considered.

For different scenes, the sets of vectors of the same object usually are not the same, since from scene to scene the object locations are changed. However, for any location the angular relationship between the vectors are stored. This fact can be used to develop invariant method of locating graphics objects. The proposed method defines the rules for building an object pattern and algorithm for its detection. The accuracy of the solution is estimated by the degree of belonging of the object to the pattern. Ideology of the algorithm is close to the methods of localization of complex

shapes based on accumulated flatness of Hough [1]. The fundamental differences relate to method of forming the accumulating rays.

Pattern creating

A pattern is a set of model characteristics of an object used for localization of the object under specified conditions of observation. To create the pattern for invariant localization of the objects in the scene are encouraged to use the following models:

model of vectorization;

model of angular spectrum;

model of corner points;

model of accumulating rays;

model of chordate lines.

Vectorization

To create a pattern a fragment of bitmap image is used, highlighting the object of interest (see fig.1). Process of object searching involves the selection of boundaries of objects, the transition to binary image boundary lines, with their subsequent presentation by a set of straight-line segments – lineaments (see fig. 2).

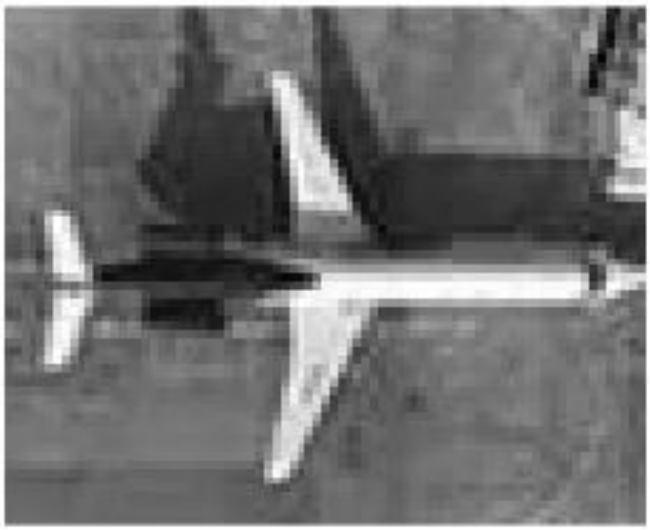

Fig. 1. Object of observation

The lineament is characterized by the angle of inclination $\alpha_i \in [-\pi/2 \div \pi/2]$ to the positive direction of the x-axis.

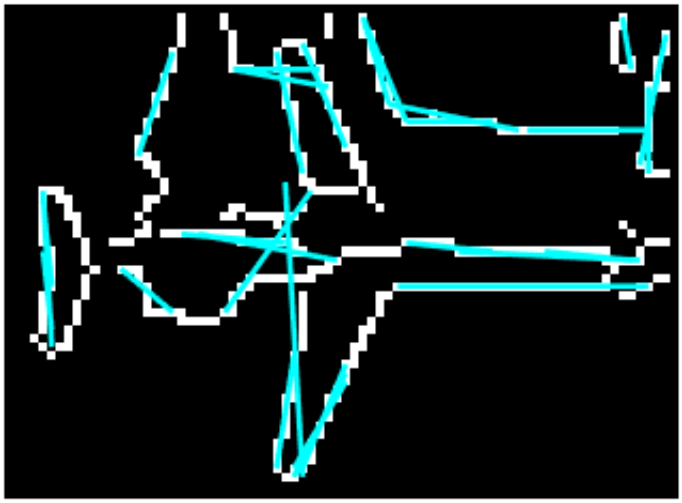

Fig 2. Vector representation of vector outlines

In our experiments the Canny method [2] was used for the selection of the edges and for building of lineaments is used classical Hough transform for lines.

Angular spectrum for pattern

The angular spectrum is determined by the set of angles between pairs of lineament belonging to an object. For the model angular spectrum of angles between lineaments are determined expressions $\omega_{ij} = |\alpha_i - \alpha_j|$. This value we call the corner detector. In the general case, the number of corner detectors is equal to the number of combinations C_N^2 where N - the number of vectors is. However, based on the requirements of precision, the angular detectors with small angles are discarded. In our experiments for thinning the angular spectrum the threshold value $\pi/6$. was used.

Corner points for pattern

For each pair of lineaments the model angular spectrum defines the corner point as the intersection of their directing lines. The terminal point of lineament the closest to the corner point is treated as the beginning of the vector, and the most remote as end (see fig. 3).

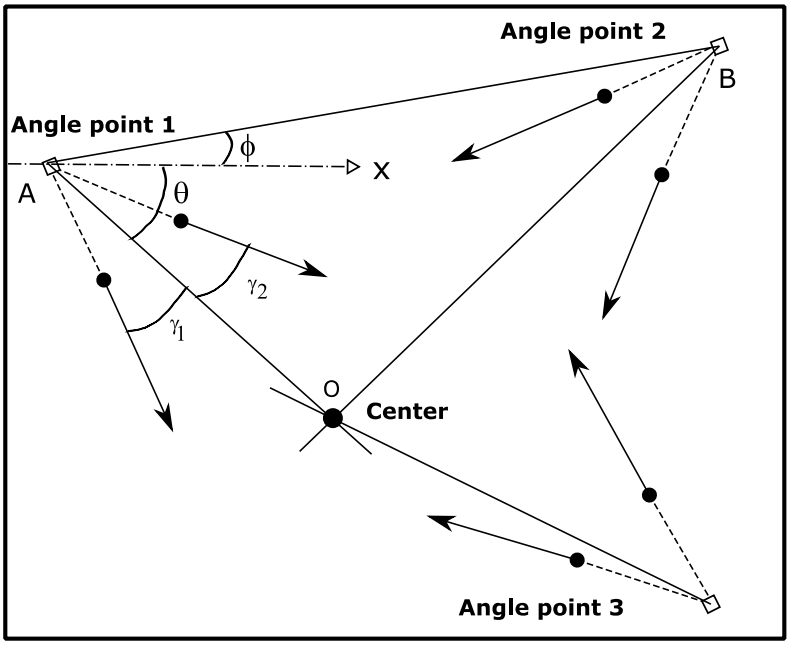

Fig. 3. Pattern model

The configuration of the set of corner points is a homomorphic mapping of object shape and their relative position is invariant to scale, rotation and linear displacement of the object.

Accumulating rays

Let us select some conditional point O for object localization. The choice of the point of localization is not unique, but in general case it can be expected that the position of a point in the center of a rectangular fragment containing the object will be minimize calculation errors. From all the corner points of the model, let us draw the rays passing through the center of the fragment (see fig. 3.) The ray is characterized by the angle $\theta \in [-\pi \div +\pi]$ to the positive direction of the axis X . Each ray gives a single brightness. We assume that for points of ray intersections these brightnesses are added. Obviously, the brightest point will be a point in the center of the fragment. The direction of the ray relative to the vectors of corner points is defined by a pair of angles $\gamma_1 = \alpha_1 - \theta, \quad \gamma_2 = \alpha_2 - \theta$.

Chord lines

Let us connect all pairs of corner points by means of linear subtending chords (fig. 3 segment AB). The chord is characterized by angle $\phi \in [-\pi \div +\pi]$ of inclination to the positive direction of the x-axis. Relatively to the directing lines of the rays, the angular position of the chord can be set by a pair of angles $\beta_1 = \theta_1 - \phi$ and $\beta_2 = \theta_2 - \phi$.

Pattern recognition

Recognition procedure represents a consistent application of pattern corner detectors to the set of vectors of the scene.

Step 1. Search for pairwise combinations of vectors of the scene which satisfy to angular spectrum $\Omega = \{\omega_{ij}\}$. The search is performed with a given angular error ($\delta = 1 \div 3$ degrees). Found pairs of vectors are candidates to belong to the pattern. Every corner pattern detector ω_{ij} is associated with the ray going from corner point to localization point of the object. For the ray, we know angle θ relative to the positive direction of the x-axis. In addition, it is known also angles γ_1 and γ_2 to determine the position of the ray relative to the pair of vectors.

Step 2. For each identified pair of vectors we determine coordinates of the corner points, and calculate actual angles α_1, α_2 . These angles with a precision equal to δ are compared with the same angles derived from the pattern ratios $\alpha_1 = \gamma_1 + \theta$ and $\alpha_2 = \gamma_2 + \theta$. In result the pairs of vectors and corresponding rays for which there is coincidence at the corners are allocated. For the selected rays it is fixed: number of corner detector, the coordinates of the corner point, the angle of the outgoing ray θ, the ordinal numbers of the vectors forming a corner point.

Step 3. The angle ϕ of the segment and the actual corners $\beta_1 = \theta_1 - \phi$, $\beta_2 = \theta_2 - \phi$ are computed for each pair of the corner points of the selected rays. These angles with a precision equaled δ are compared with the same corners of the

pattern. With corresponding the angles, the rays are considered as true rays. For the true rays the points of intersection with the other true rays, (which were accumulated previously) are determined. The intersection points are accumulated. The true rays are accumulated also.

Step 4. After step 3, the coordinates of the intersection points are rounded to one pixel. The point of intersection into the accumulating plane is assigned a single brightness. The brightness of the points with equaled coordinates are added. When the correct pattern is recognized, the point with the maximum brightness will obviously correspond to the localization point of the object. The reliability of the obtained solutions can be evaluated by comparing the brightness of the discovered localization point with brightness of the same point in pattern.

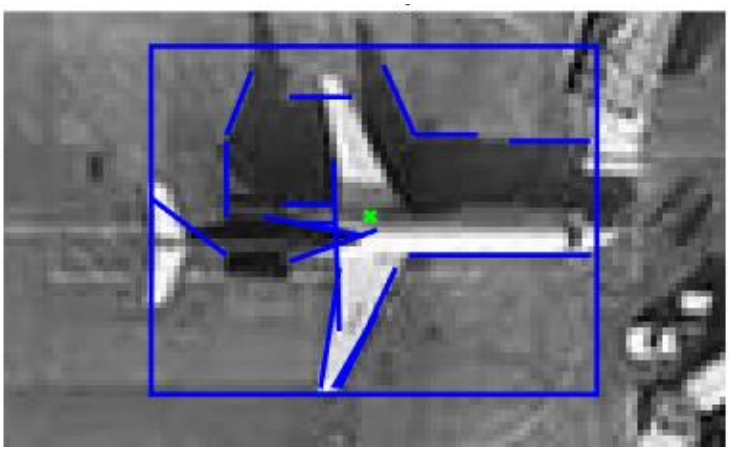

Fig. 4. Object locating

Bounding rectangle

The final stage of object localization is associated with the building for the minimum bounding a rectangle with sides parallel to the coordinate axes.

Construction is expressed in determination of coordinates of the terminal points of the found object vectors and the most remote from its point of localization.

The ordinal numbers of the vectors forming the corner points, and presumably belonging to the object are contained in description of the true rays. The test for vectors on membership to the object is in calculation of actual angle of the directing line for each ray. This can be done by knowing the coordinates of the corner points

and the point of localization of the object when a pattern is recognized. The actual angle with an accuracy δ is compared with angle of the pattern stored in the description of the ray when it is created. If values coincide, the pair of vectors forming the ray is considered reliable. For set of reliable vectors, the minimum and maximum coordinate values of vector terminal points are determined. Finally, the resulting coordinates of the rectangle are symmetrized relative to the of localization point of the object. In Fig. 4 shows the results of localization of the object in the scene.

Conclusion

The proposed method of invariant localization of objects for scene contains phases of training and recognition. The learning phase it is created a pattern model, and the phase of recognition the problem of object localization is decided.

The method allows to determine the point of localization of the object and the coordinates of the bounding rectangle with the assessment of the reliability of the solution. The results of the experiments on real images confirm the effectiveness of the proposed method.

References

1. Обработка и анализ изображений в задачах машинного зрения. Визильтер Ю.В., Желтов С.Ю. Бондаренко А.В., Осоков М.В., Моржин А.В. – Курс лекций и практических занятий. – М.: Физматкнига, 2010. – 672с.
2. Canny, John, "A Computational Approach to Edge Detection," IEEE Transactions on Pattern Analysis and Machine Intelligence,Vol. PAMI-8, No. 6, 1986, pp. 679-698.

УЛУЧШЕНИЕ ПРОСТРАНСТВЕННОГО РАЗРЕШЕНИЯ ВИДЕОКАДРОВ ДЛЯ ПОВЫШЕНИЯ ЭФФЕКТИВНОСТИ КЛАССИФИКАЦИИ ИЗОБРАЖЕНИЙ

Луцив Вадим Ростиславович

доктор. техн. наук, профессор Университета ИТМО, г. Санкт-Петербург

E-mail: vluciv@mail.ru

Малашин Роман Олегович

канд. техн. наук, научный сотрудник Института физиологии им И.П. Павлова, Санкт-Петербург

E-mail: malashinroman@mail.ru

Недошивина Любовь Сергеевна

магистрант Университета ИТМО, Санкт-Петербург

E-mail: nedshivina@gmail.com

ENHANCING THE SPATIAL RESOLUTION OF VIDEO FRAMES FOR INCREASING THE EFFICIENCY OF IMAGE CLASSIFICATION

Lutsiv Vadim

Doctor of Science, professor of ITMO University, Saint Petersburg

E-mail: vluciv@mail.ru

Malashin Roman

Candidate of Science, scientific associate at the Pavlov Institute of Physiology, Saint Petersburg

E-mail: malashinroman@mail.ru

Nedoshivina Lubov'

undergraduate of the ITMO university

E-mail: nedshivina@gmail.com

АННОТАЦИЯ

Описан метод повышения пространственного разрешения единственного снимка в формате Байера. Используется взаимное смещение цветовых слоев в снимке вместо смещения изображений в последовательных кадрах, а R, G и B компоненты в цветовом субпикселе Байера восстанавливаются с учетом локальной взаимной коррелированности цветовых слоев. Таким образом, изменения в последовательных кадрах не влияют на результаты повышения разрешения. Дополнительная информация восстанавливается при повышении разрешения, поэтому оно использовано для увеличения надежности анализа снимков, полученных при плохом освещении.

ABSTRACT

A method is presented for increasing the spatial resolution in single Bayer frame. Mutual displacement of color layers in Bayer-encoded image is applied instead of displacement of several frames and the R, G, and B components of color sub-pixels in Bayer cell are restored based on local mutual correlation of color layers. Thus, no changes in sequential frames interfere with increase of resolution. Additional information is restored by increasing of resolution, thus it is considered as a tool for enhancing of automatic object classification in the video-frames acquired at poor illumination.

Ключевые слова: супер-разрешение; формат Байера; цветовой слой; смещение изображений; коррелированность цветовых слоев; автоматический анализ изображений.

Keywords: super-resolution; Bayer’s format; color layer; images displacement; correlation of color layers; automatic image analysis.

Introduction

Increase of image spatial resolution is important both for enhancing of image visual quality and for more reliable functioning of diversified automatic image analysis algorithms. One of the most widely used methods for solving this task is application of variational algorithm TVL (total variation with L metric) practically applied and described in detail in many papers (see e.g. in [1]). This algorithm applies a joint analysis of several initial mutually spatially transformed images of low spatial resolution and iteratively restores the pixel intensities of higher spatial resolution image by minimization of total difference between the initial images and the restored one. The solution is reached by gradient descent using the following incremental changes of restored (not degraded) higher spatial resolution image $\underline{\hat{\boldsymbol{X}}}_{n+1}$ presented in vector form:

$$\underset{--n+1}{\hat{\boldsymbol{X}}} = \underset{--n}{\hat{\boldsymbol{X}}} - \beta\left[\sum_{k=1}^{N} \boldsymbol{F}_k^T \boldsymbol{H}_k^T \boldsymbol{D}_k^T \operatorname{sign}\left(\boldsymbol{D}_k \boldsymbol{H}_k \boldsymbol{F}_k \underset{--n}{\hat{\boldsymbol{X}}} - \underset{--k}{\boldsymbol{Y}}\right)\right.$$
$$\left. + \lambda \sum_{l=0}^{P} \sum_{m=0}^{P} \alpha^{m+l} \left(\boldsymbol{I} - \boldsymbol{S}_y^{-m} \boldsymbol{S}_x^{-l}\right) \operatorname{sign}\left(\underset{--n}{\hat{\boldsymbol{X}}} - \boldsymbol{S}_x^{l} \boldsymbol{S}_y^{m} \underset{--n}{\hat{\boldsymbol{X}}}\right)\right], \quad (1)$$

where n a is sequential number of iteration, $\underline{\boldsymbol{Y}}_k$ is a k-th degraded image of low spatial resolution presented in vector form (k=1, …, N), $\boldsymbol{D}_k$, $\boldsymbol{H}_k$ and $\boldsymbol{F}_k$ are respectively the matrix operators of pixels decimation (decrease of spatial resolution), image defocus and geometric transformation. $\boldsymbol{S}_x^{\,l}$ и $\boldsymbol{S}_y^{\,m}$ are the matrix operators of translations along abscissa and ordinate axes by l and m pixels respectively applied for calculation of brightness derivatives. P is the maximum order of brightness derivative to be taken into account in the restored image of higher resolution. $\alpha \in (0;1)$ shows the decrease velocity for the contribution of higher order derivatives into regularization term (the second line in the formula (1)), and λ shows the weight of regularization term. $\boldsymbol{I}$ is the identity matrix and β is the velocity of gradient descent.

Theoretical background

There could be a case when the set of spatially displaced initial images of low resolution is acquired at the same moment by several cameras having differing spatial positions. However, in this paper the case of single camera is of primary interest. In such case, a set of initial images is usually acquired by slightly rotated or shaking camera in sequential time moments. Unfortunately, in this situation, the additional difficulties appear when dealing with dynamically changing scenes containing separately moving objects. Thus, we discuss here an alternative approach proposed in [2, 3] by Kanaev et al, that allows acquiring several mutually displaced images at the same moment.

This approach is based on the properties of Bayer-encoding widely applied in modern cameras. In particular, the "layers" of red, green, and blue subpixels in the "color cells" of Bayer-encoded image are mutually displaced in one or two directions by half of size of color cell (composed usually of red, blue, and two green neighboring subpixels). Thus, these red, blue and two green "color layers" could be considered as mutually displaced images of the same scene, acquired at the same single time moment. We will get in this way four initial images $\underline{\boldsymbol{Y}}_k$ (k=1, …, 4) to be substituted into formula (1). However, each of these color layers contains a monochrome image while the red, green, and blue color components should be available at every pixel in each of these four mutually displaced images for restoring a color image of higher spatial resolution using the mentioned above TVL[1] algorithm. The missing color components are usually calculated for each monochrome Bayer subpixel by special (e.g. bilinear) interpolation based on the intensities of neighboring subpixels of respective color in the Bayer-encoded sensor matrix. However, any kind of such interpolation cannot restore 100% of information lost in the pixels being interpolated, and the larger is the Bayer cell (there also can be the cells of 3×3 or 4×4 subpixels in size [3]), – the longer is the pixel sequence to be restored and the lower will be interpolation quality.

However, in the color RGB photographs of natural scenes, the content of color layers is strongly locally correlated [2, 3]. On the one hand, the pass band of color filters attached to subpixels of Bayer cells strongly overlap, as it is shown in the fig.1. On the other hand, the borders of the same object are usually located at the same places in different color bands, as it is illustrated in the fig.2.

Due to this inter-color correlation, the pixels of one color layer of Bayer-encoded image may make contribution into calculation of higher resolution for another color layer according to formula (1), but this contribution should be proportional to local mutual correlation of these color layers. Thus, the formula (1) will be transformed to formula (2) in which the factor $U_{r,k}$ takes into account the correlation of local content of color layer number k (k=1, …, 4 respectively for the red, green, blue, and green color subpixels composing Bayer's color cell) with the local content of color layer number r for which the higher spatial resolution is being restored. The spatial transforms $\boldsymbol{F}_k$ are reduced in this case to displacements along the abscissa or/and ordinate axes by half of step between neighboring Bayer cells.

$$\underset{--n+1}{\hat{\boldsymbol{X}}} = \underset{--n}{\hat{\boldsymbol{X}}} - \beta\left[\sum_{k=1}^{4} \boldsymbol{F}_k^T \boldsymbol{H}_k^T \boldsymbol{D}_k^T \operatorname{sign}\left(\boldsymbol{D}_k \boldsymbol{H}_k \boldsymbol{F}_k \underset{--n}{\hat{\boldsymbol{X}}} - \underset{--k}{\boldsymbol{Y}}\right) U_{r,k} + \lambda \sum_{l=0}^{P} \sum_{m=0}^{P} \alpha^{m+l} \left(\boldsymbol{I} - \boldsymbol{S}_y^{-m} \boldsymbol{S}_x^{-l}\right) \operatorname{sign}\left(\underset{--n}{\hat{\boldsymbol{X}}} - \boldsymbol{S}_x^{l} \boldsymbol{S}_y^{m} \underset{--n}{\hat{\boldsymbol{X}}}\right)\right]. \quad (2)$$

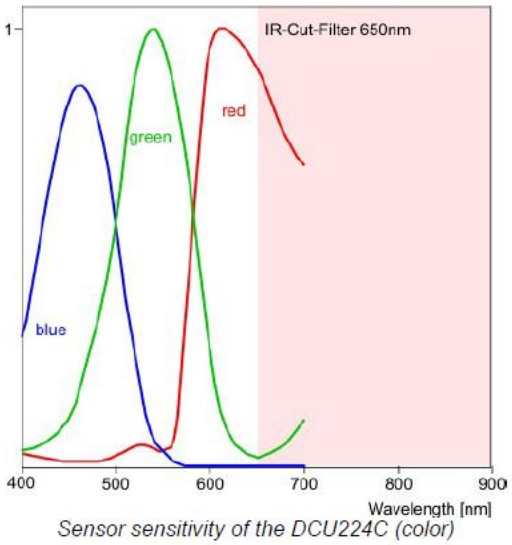

Figure 1 – Overlapping pass bands of color filters in the modern cameras

a b c d

Figure 2 – Images of blue (a) and green (c) color layers of the same RGB image and the contours (b and d) of object borders detected in them by Hildreth-Marr filtering

Kanaev et al proposed to calculate the factor $U_{r,k}$ as

$$U_{r,k} = \exp\{-(C_{r,k}-1)^2 / a\}, \qquad r,k = 1...4, \tag{3}$$

where r and k are the sequential numbers of Bayer's color layers, a is a free parameter taking into account the degree of similarity of Bayer's color layers, and $C_{r,k}$ is the local coefficient of correlation of respective pixels in the r-th and k-th color layers to be calculated using the formula (4):

$$C_{A,B} = \frac{\sum_i \sum_j \left(A_{i,j} - \overline{A}\right)\left(B_{i,j} - \overline{B}\right)}{\sqrt{\left[\sum_i \sum_j \left(A_{i,j} - \overline{A}\right)^2\right] \cdot \left[\sum_i \sum_j \left(B_{i,j} - \overline{B}\right)^2\right]}} \tag{4}$$

in which $A_{i,j}$ $B_{i,j}$ are the i-th and j-th pixels in A and B image layers, respectively, and $\overline{A}, \overline{B}$ are the average brightness in these layers within a chosen local region of homogeneous color. The homogeneous regions were proposed to be selected by k-means clustering of RGB color vectors.

Results of practical investigation

We practically investigated the described above technique. An example of experimental color image and selected in such way homogeneous regions is

presented in the fig.3. It was proposed in [2] to use 15 or 20 clusters but we found experimentally that 10 clusters were sufficient. We also found in our experiments that the factor $U_{r,k}$ is calculated inefficiently with the use of formula (3). The function (3) is of the form of Gaussian "bell" having the regions of extremely small slope, and it is not sensitive in such regions to changes in mutual correlation of Bayer's color layers. Thus, we replaced this function with a linear one of the form (5). With a suitable experimentally found value of free parameter a=0.2, this modification turned out to be successful.

$$U_{r,k} = \max\{(a\ C_{r,k} - a + 1),\ 0\}. \qquad (5)$$

For the example of experimental image presented in the fig.3, the initial Bayer's color layers from which this image was interpolated are shown in the fig.4. It was mentioned in [3] that the discussed technique can cause come local color distortions. An example of initial image of low spatial resolution and an image of increased resolution restored from it in [3] are shown in the fig.5. Some color distortions are really visible. A similar effect can be found in our own result shown in the fig. 6.b. A substantial color noise and distortion of color hues is can be seen.

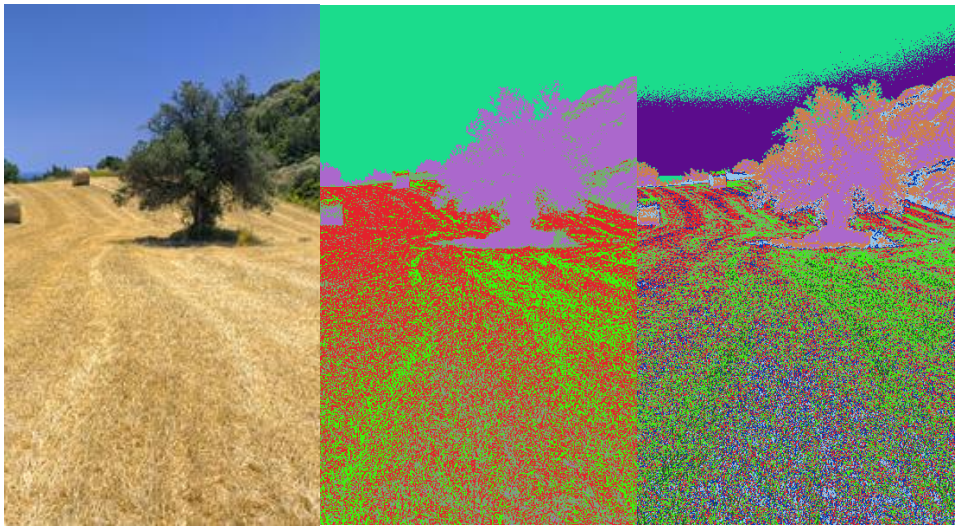

a b c

Figure 3 – Initial color image (a) and the results of image separation into regions of homogeneous color by k-means clustering of RGB color into 5 (b) and 10 (c) clusters

a b c d

Figure 4 – The first green (a), blue (b), red (c), and second green (d) Bayer's color layers from which the color image shown in the fig.3.a was interpolated

We solved this color distortion problem using a pansharpening algorithm in the following way. It could be noticed that the color distortions mentioned above change the color hue, but they do not affect pixel brightness in general. Thus, we converted the restored color image of higher spatial resolution to grey tone mode and then colored the grey tone pixels with the colors taken from a color image interpolated from Bayer's color layers by usual (e.g., bilinear technique). Thus, the brightness variation of high resolution image was retained while the spatial resolution of color hue changes was lost to some extent with is not so crucial for human perception and is widely applied, e.g., in the JPEG compression algorithm.

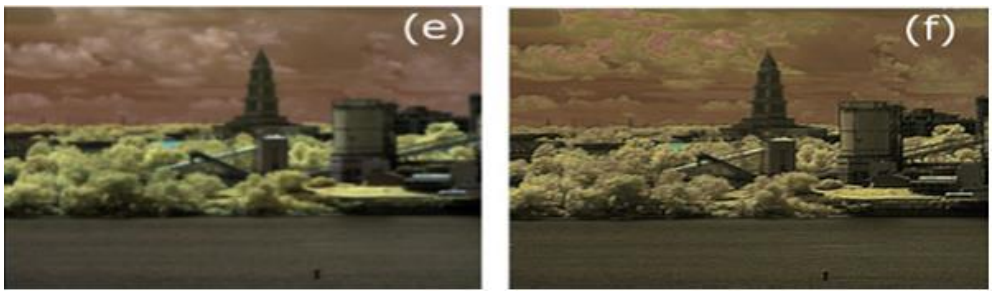

a b

Figure 5 – Initial image of low spatial resolution interpolated from Bayer's format and image of increased resolution restored from it by Kanaev at al [3]

Conclusion

We demonstrated above a resolution increase possibility for a single Bayer-encoded imag, which is especially important for single cameras observing the moving objects. In further research, we will investigate the possibilities of increasing the reliability of object recognition in result of such enhancement of image resolution. It seems to be possible because Kanaev at al successfully applied such increase of resolution in [2] (section 4.B) and [3] (section 4) for enhancing the reliability of target recognition despite color distortions resulting from application of the proposed technique. In particular, we would like to get sure that such image preprocessing could be useful in automatic analysis of images acquired at poor illumination. A joint tuning of sequentially applied image preprocessing and image classification algorithms could be in this case an additional important area of investigation.

Acknowledgements

We are thankful to Mr. Alexander Kadykov for his help in application of pansharpening algorithm. We also thank Samsung R&D Institute for kind supporting this investigation.

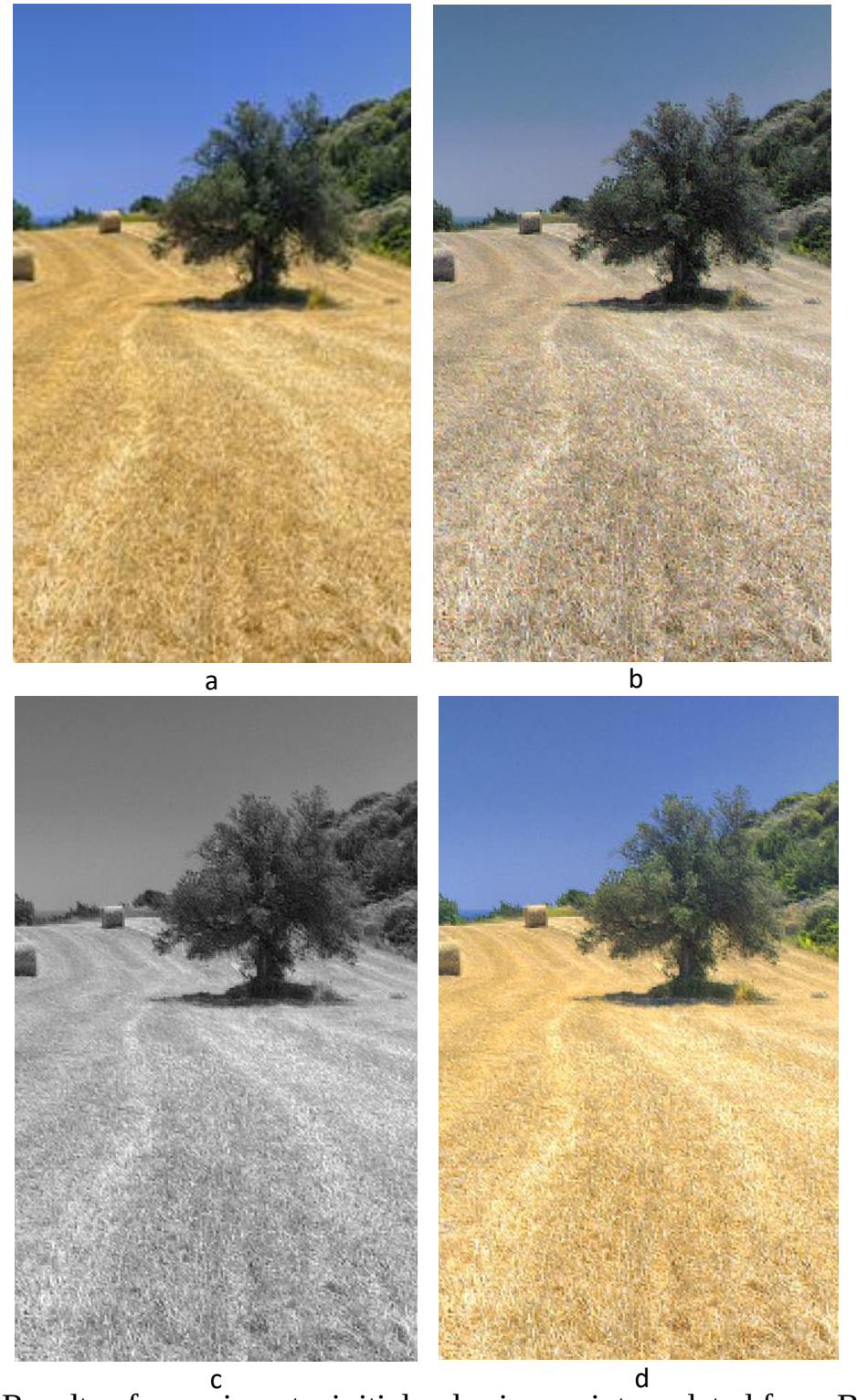

Figure 6 – Results of experiments: initial color image interpolated from Bayer format (a), restored color image of enhanced spatial resolution (b), restored image converted to grey tone mode (c), grey tone image colored by pansharpening algorithm (d)

References

1. S. Farsiu, D. Robinson, M. Elad, P. Milanfar. Fast and robust Super-Resolution. Proc 2003 IEEE Int Conf on Image Process, pp. 291–294, 2003.
2. Kanaev, A. V., Kutteruf, M. R., Yetzbacher, M. K., Deprenger, M. J., Novak, K. M. Imaging with multi-spectral mosaic-array cameras // Applied Optics. 2015. V. 54. P. F149-F157.
3. Kanaev A. V. Compact full-motion video hyperspectral cameras: development, image processing, and applications // Proc. of SPIE. 2015. V. 9649, P. 96490R1-96490R7.

СОВРЕМЕННЫЕ НАПРАВЛЕНИЯ, МЕТОДЫ И ВЫСОКОЭФФЕКТИВНЫЕ РЕШЕНИЯ КОМПАНИИ «ТРИМ СШП ИЗМЕРИТЕЛЬНЫЕ СИСТЕМЫ» В ОБЛАСТИ ИЗМЕРЕНИЯ АНТЕННЫХ РЕШЕТОК

Миляев Анатолий Павлович

главный конструктор, «ТРИМ Сверхширокополосные измерительные системы», г. Санкт-Петербург

E-mail: anatoly.milyaev@gmail.com

Калинин Юрий Николаевич

Кандидат технических наук, заместитель генерального директора по научной работе, «ТРИМ Сверхширокополосные измерительные системы», г. Санкт-Петербург

E-mail: kalinin@trimcom.ru

Савченко Даниил Игоревич

программист, «ТРИМ Сверхширокополосные измерительные системы», г. Санкт-Петербург

E-mail: cfdx@list.ru

MODERN TRENDS, METHODS AND PROBLEMS IN ANTENNA ARRAYS MEASUREMENTS AND LOW COST/HIGH PRECISION SOLUTIONS BY «NPP TRIM UWB MEASUREMENT SYSTEMS»

Milyaev Anatoly Pavlovich,

Director of Engineering, «TRIM UWB Measurement systems», Saint-Petersburg

E-mail: anatoly.milyaev@gmail.com

Kalinin Yurii Nikolaevich,

Ph.D, Chief research officer,

«TRIM UWB Measurement systems», Saint-Petersburg

E-mail: kalinin@trimcom.ru

Savchenko Daniil Igorevich

Software developer, «TRIM UWB Measurement systems», Saint-Petersburg

E-mail: cfdx@list.ru

АННОТАЦИЯ

Рассматривается одна из главнейших частей современных комплексов для проверки параметров фазированных антенных решеток – комплексное специализированное программное обеспечение, обеспечивающее управление оборудованием, сбор и каталогизацию данных, интерфейс пользователя. Показана структура, составные части, функциональные возможности и основной инструментарий нового программного обеспечения, входящего в состав автоматизированных измерительно-вычислительных комплексов ООО «НПП «ТРИМ СШП Измерительные системы».

ABSTRACT

The article will focus on one of the most essential parts of modern measuring and computing facility for antenna array testing - integrated specialized software package - applicable for control of equipment, collection and handling of data, operator's interface.

Careful consideration is given to structure, elements, functional capabilities and the essential instrumentation of a new software which is a part of automated measuring and computing facility developed by «TRIM UWB Measurement systems» company .

Ключевые слова: измерения параметров антенн, антенные решетки, программное обеспечение.

Keywords: antenna parameters measurement, antenna arrays measurement, software.

Today one cannot imagine the exchange of information without using wireless device. And every such device contains antenna or antenna facility: either mobile phone or operator base station. Both range and speed of communication depend directly on quality of antenna calibration. To solve this task TRIM company suggests a fully automated measuring and computing facility for antenna calibration in laboratory.

The most important part of modern automated measuring and computing facility for antenna measurements is a software. A new software package is developed by «TRIM UWB Measurement system» company which is intended for measurements, calculations and visualization of antenna parameters. This software package provides the capability for measurement scenarios, calculations, data processing and visualization of results for a large scope of measurements, including:

a) cuts and volume patterns in far field;

b) antenna measurements in near field (planar, cylindrical and spherical scanning), including measurements of gain by various methods;

c) gain, polarization characteristics, effective isotropically radiated power measured by various ways in far field.

Software structure consists of the following elements (Figure 1):

MeasurementCentre program, data base, ProViLab program for calculation and visualization of measurement results.

MeasurementCentre program provides the possibility for measuring process itself, monitoring and alignment of equipment. Measurements are conducted under formalized scenarios which may be determined as well by TRIM's engineers, as the qualified specialists of the Customer. It helps to simplify and automatize maximally the operating process and to keep the opportunity for non-standard measurements.

ProViLab program is a modern CAD (see Figure 2) applicable to calculation, analyses and visualization of the measuring data, to generation of reports and to working out a large range of additional engineering issues related to processing treatment. The main program tools is a set of highly integrated means for visualization and calculation, providing the capability to solve non-trivial research and automation tasks.

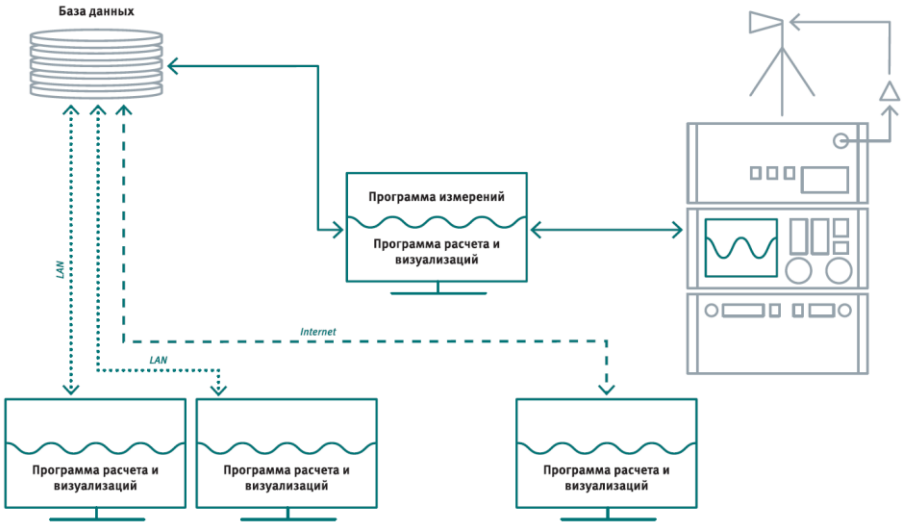

Figure 1 – structure of software package

Among the particulars of this program may be highlighted the following:

a) a convenient user's interface for interactive handling of calculations and visualization directly from graphic pictures;

b) high speed of calculations, rapid receipt of results while data processing;

c) support of random composition of display and print forms, simplicity of report generation;

d) a capability of using a report as a template for measurements of the same type, a capability to automatic changing of measuring in a whole report;

e) a wide range of 2D and 3D visualization and calculation tools, easily configurable visualization.

f) a wide range of tools for research, comparison and transformation of plots and patterns.

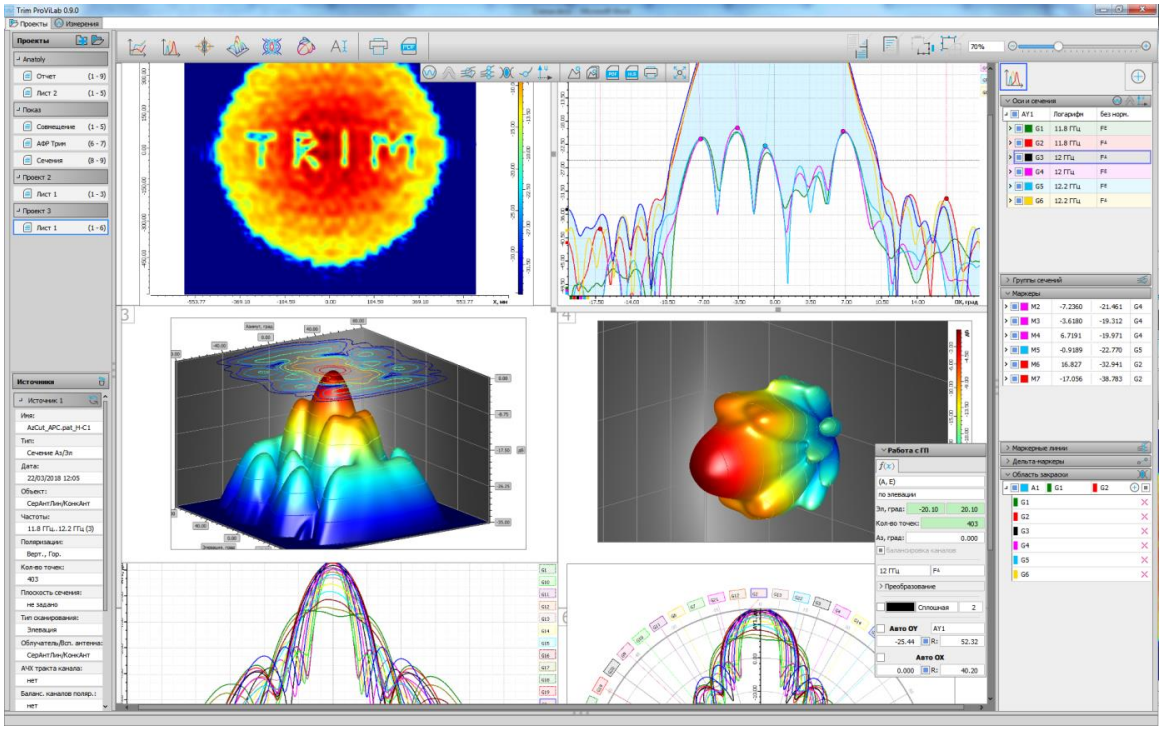

Figure 2 – screenshot of ProViLab program

The software structure under consideration provides:

a) a clear interaction between system parts: measurement results obtained using MeasurementCentre program are at once accessible for display and calculation in ProViLab program;

b) a capability for various configurations of network: starting from one workplace with all software elements installed up to a situation when a lot of operators simultaneously work at a various workstations using ProViLab program;

c) a modern relational system for database management which provide a reliable storage of great volume of information. Meanwhile software package includes advanced tools for automation of work with lists of done measurements, objects of measurement, probes, reference antennas and etc. In particular, the functions of search/filtration and dynamic hierarchical data grouping in accordance with different attributes (type of measurement, objects of measurement, date, operator, operator's definitions, etc.). Therefore, it is not difficult to find a required measurement even among thousands of measurements in a database.

In the context of measurement support MeasurementCentre program provides:

a) automated and interactive step-by-step measuring;

b) automatic formation of executed algorithms for measurements of diverse types;

c) use of various type of radio and mechanic equipment of own developed and of world producers;

d) tech support of typical process, for example, search of pattern maximum, tract amplitude-frequency performance, calibration, manual control of positioner motion, signal monitoring and etc.;

e) visual creation of circuit diagrams of equipment;

f) creation and keeping of ready-for-use measurement templates.

Algorithmic support in ProViLab program is based on advanced achievements described in world scientific literature on antenna measurements [1, 2], and on TRIM's own working-outs [3, 4]. In this context we focus attention on the following possibilities:

a) calculation and visualization of volume patterns and pattern cuts in various coordinate systems ((A, E), (α, ε), (θ, φ), (k^x, k^y)) and polarization bases (Ludwig-I, Ludwig-II, Ludwig-III, circular);

b) calculation of amplitude-phase distribution in antenna aperture and at a random distance from scanning plane [3];

c) automatic calculation of antenna parameters (polarization characteristic, gain, phase center coordinates [4], pattern width at a given level, antenna boresight).

For working with pattern cuts and plots in ProViLab program, the advanced tools with two-dimensional design are realized (Figure 3), including:

a) calculation, visualization and analysis of pattern cuts, amplitude-phase distribution, gain, polarization characteristic, directive gain, amplitude-frequency characteristic, time signals, spectrum and etc.;

b) wide and good opportunities for transformation and analysis of cut, including arithmetic calculation, Fourier transformation, window functions, smoothing/ filtration, interpolation, transformation of measurement units, statistical processing;

c) specialized visualization for work with pattern cuts, in Cartesian coordinates and in polar coordinates;

d) simple and intuitive control of arbitrary groups of plots and cuts (selection of frequency, polarization, types and parameters of both calculation and transformation);

e) markers with function of search for local and global extremum, given values, relation with other markers;

f) marker lines, delta lines between markers, customizable fill areas, display of legends and etc.

ProViLab program provides a great number of 3D visualization tools (Figure 4), 3D patterns, polarization characteristic, for:

a) creation of spectrogram and axonometric projections, visual representation by lines of different level;

b) possibility of interactive setting the arbitrary cuts of 3D-surface;

c) a convenient instrumentation tools for markers, automatic search of local and global extremum;

d) support of joint visualization and processing of several 3D-surfaces, including averaging, construction of differences and ratio of surfaces, scatter, imposition of several patterns (for example, different beams);

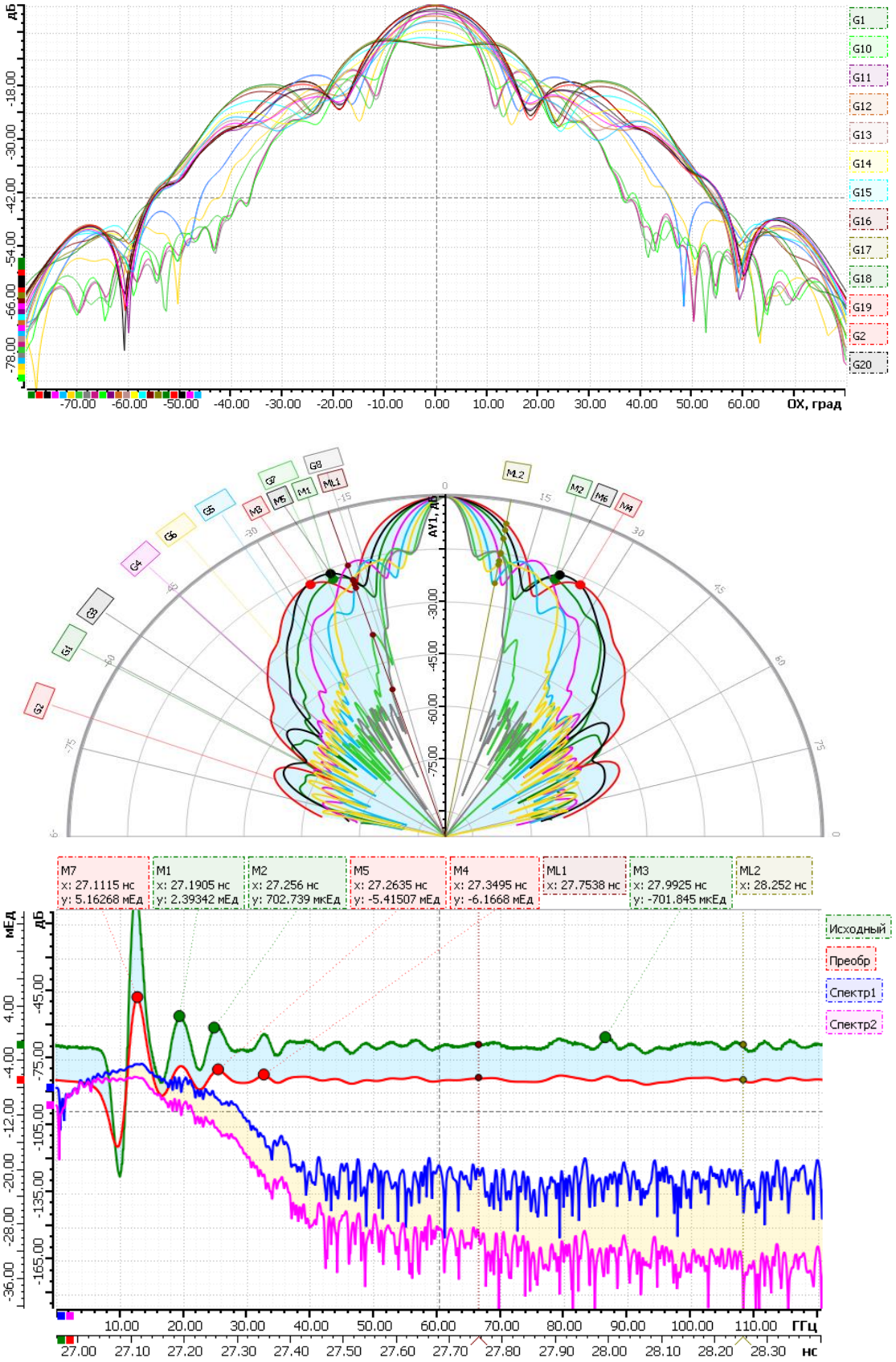

Figure 3 – 2D-visualization in ProViLab program

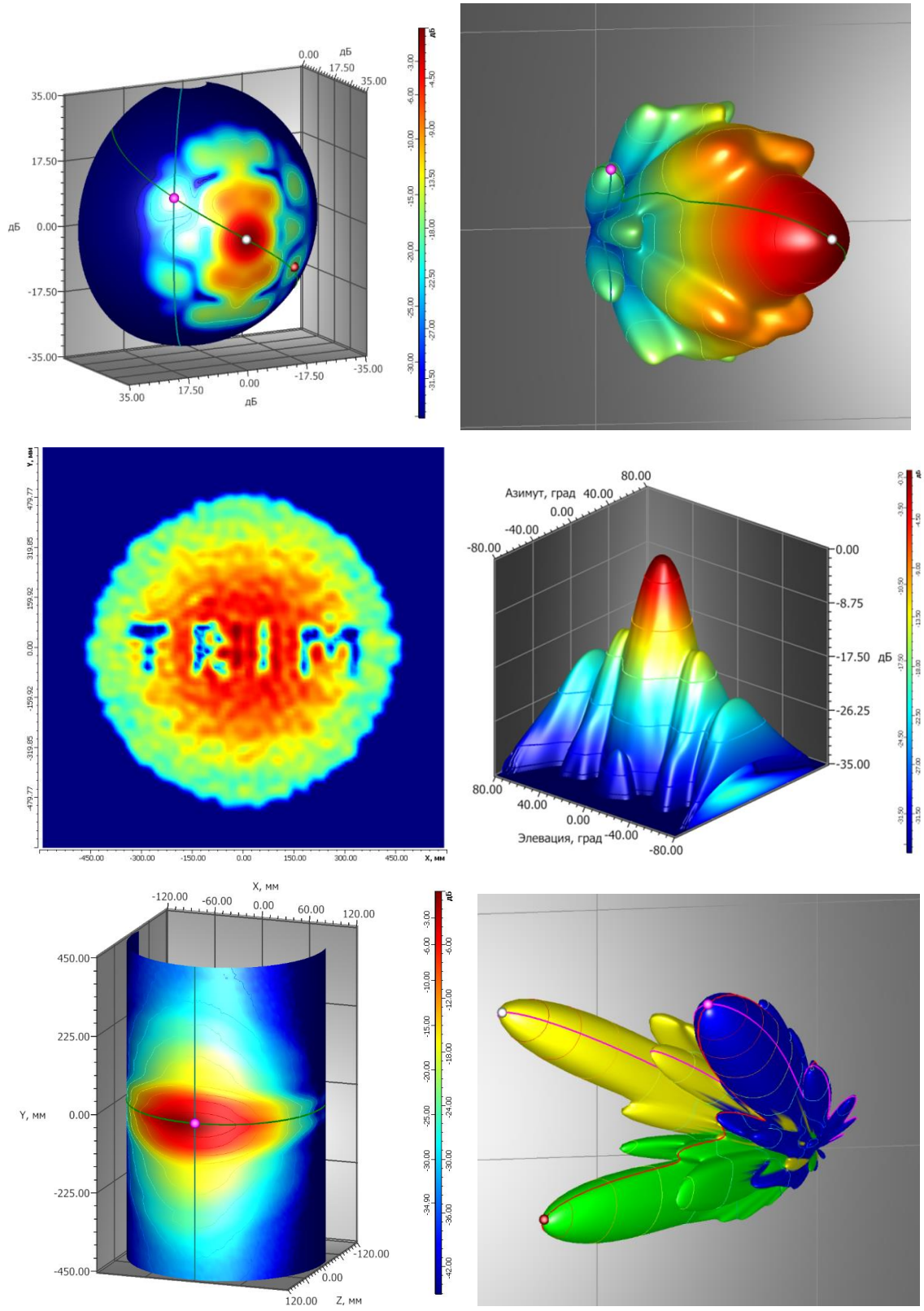

Figure 4 – 3D-visualization in ProViLab program

e) a wide range of opportunities of visual settings, (same level lines, gradient control, fill setting modes, mesh display and etc.).

Among the other characteristics of software developed by TRIM company may be considered:

a) possibility of translation of display interface into various languages and adaptation upon regional standards,

b) possibility of measurement, data proccesing and visual view of results using «hidden frequency»;

c) founded at the design stage modular architecture, it provides a possibility for functional development and adaptaion of software in accordance with the specific requirements of the Customer;

d) export of visual pictures, measurement results and calculations into different external formats (GRASP, xls, txt, pdf, png, jpeg and etc.).

The usage of TRIM software helps to speed up the serial antenna calibration and to systematize the results of the experiments for developing prototypes of new devices. That in its turn helps to speed up the process of developing new antenna products.

Bibliography:

1. IEEE Recommended Practice for Near-Field Antenna Measurements. – Antenna Standards Committee of the IEEE Antennas and Propagation Society, IEEE Std 1720 – 2012.

2. Parini C., Gregson S., McCormic J., Daniel J. Theory and Practice of Modern Antenna Range Measurements (Electromagnetic waves series, v.55). – London. Institution of Engineering and Technology. – 2015.

3. Kalinin Yurii, Measurement of antenna pattern using planar scanner without phase measurement // Antennas. – 2015. – №1. – page 61-68.

4. Kalinin Yurii, Measurement of coordinates of antenna phase center. // Antennas. – 2014. – №4. – page 54-62.

НОВЫЕ НОСИТЕЛИ ЗАДАЧИ СКРЫТОГО ДИСКРЕТНОГО ЛОГАРИФМИРОВАНИЯ ДЛЯ ПОСТКВАНТОВОЙ КРИПТОГРАФИИ

Молдовян Александр Андреевич

д-р техн. наук, профюр, главный научный сотрудник лаборатории безопасности информационных систем Санкт-Петербургский институт информатики и автоматизации Российской академии наук), г. Санкт-Петербург

E-mail: maa1305@yandex.ru

Молдовян Николай Андреевич

д-р техн. наук, профюр, главный научный сотрудник лаборатории безопасности информационных систем Санкт-Петербургский институт информатики и автоматизации Российской академии наук), г. Санкт-Петербург

E-mail: nmold@mail.ru

NEW CARRIERS OF HIDDEN LOGARITHM PROBLEM FOR POST-QUANTUM CRYPTOGRAPHI

Alexandr Moldovyan

Ph.D., Professor, Chief Researcher of Lab. of Inform. Systems Security, St. Petersburg Institute for Informatics and Automation of Russian Academy of Sciences (SPIIRAS)

Nikolay Moldovyan

Ph.D., Professor, Chief Researcher of Lab. of Inform. Systems Security, St. Petersburg Institute for Informatics and Automation of Russian Academy of Sciences (SPIIRAS)

АННОТАЦИЯ

Предлагаются новые варианты задания задачи дискретного логарифмирования в скрытой группе, которая представляет интерес Для построения постквантовых криптографических протоколов и алгоритмов, основанных на задаче дискретного

логарифмирования в скрытой группе, предлагаются новые конечные ассоциативные алгебры в качестве носителей указанной задачи. Предложенные алгебры обладаю существенно различными свойствами в сравнении с конечной алгеброй кватернионов, над которой ранее была сформулирована скрытая задача логарифмирования. Предложены новые варианты формулировки указанной задачи.

ABSTRACT

There are introduced novel finite associative algebras as carriers of the discrete logarithm problem in a hidden group, which represents interest for constructing post-quantum cryptographic protocols and algorithms. The introduces algebras possess significantly different properties than quaternion algebra over which the hidden logarithm problem was earlier formulated. New forms of defining the last problem have been proposed.

Ключевые слова: шифры с открытым ключом, постквантовые криптосхемы, задача дискретного логарифмирования, конечные алгебры

Keywords: public-key ciphers, post-quantum cryptoschemes, discrete logarithm problem, finite algebras.

The public-key cryptographic algorithms and protocols are widely used for solving different security problems of the information and telecommunication technologies. A large part of such cryptoschemes is based on the following two computationally difficult problems: factorization and finding discrete logarithm. However each of these two problems can be solved on a quantum computer in polynomial time [1,2]. One of actual challenges in the area of cryptology is development of the public-key cryptoschemes that are secure to attacks based on using quantum computers [3].

One of attractive post-quantum primitives is the hidden logarithm problem (HLP). This problem was earlier defined over finite non-commutative associative algebras [4,5]. Proposed in the literature post-quantum cryptoschemes are based on the HLP defined over finite quaternion algebra [6]. Detailed study of the HLP in finite quaternion algebra defined over the finite field $GF(p)$ [7] had shown that the HLP can be reduced to the problem of finding discrete logarithm in $GF(p^2)$. To design post-quantum cryptoschemes on the base of the HLP in paper [7] it had been proposed to look for other carriers of the HLP.

In present paper there are introduced new 4-dimensional finite non-commutative associative algebras (FNAAs) as carriers of the HLP, which possess different properties. Some of the introduced algebras contain only local unit elements therefore there are proposed new forms of defining the HLP which are different from the form considered in [6,7]. There is also proposed a general method for defining FNAAs of an arbitrary dimension $m > 1$.

Suppose $\mathbf{e}_i$, where $i = 0, 1, \ldots, m$ 1, are some formal basis vectors and $v_i \in GF(p)$, where p is a prime, are coordinates of the vectors V contained in the m-dimensional vector space. Such vector space with associative multiplication operation added to the usual scalar-multiplication and addition operations represents the m-dimensional FNAA over $GF(p)$. Multiplication of two vectors A and B is defined as follows:

$$A \circ B = \left(\sum_{i=0}^{m-1} a_i \mathbf{e}_i \right) \circ \left(\sum_{i=0}^{m-1} b_i \mathbf{e}_i \right) = \sum_{i=0}^{m-1} \sum_{j=0}^{m-1} a_i b_i \left(\mathbf{e}_i \circ \mathbf{e}_j \right), \quad (1)$$

where $\circ$ denotes multiplication operation of two vectors and products of all possible pairs of the basis vectors are to be replaced by some single-component vectors in accordance with so called basis-vector multiplication table (BVMT). Coordinates of the single-component vectors contained in BVMT are called structural coefficients. Constructing a BVMT defining an associative multiplication operation means constructing a particular FNAA. Some 4-dimensional FNAAs are the following ones.

Four-dimensional FNAA with global unit is defined by the BVMT shown as Table 1.

Table 1.

Defining a 4-dimensional FNAA with global unit

$\circ$	$\mathbf{e}_0$	$\mathbf{e}_1$	$\mathbf{e}_2$	$\mathbf{e}_3$
$\mathbf{e}_0$	$\mathbf{e}_0$	$\alpha\mathbf{e}_3$	$\alpha\mathbf{e}_0$	$\mathbf{e}_3$
$\mathbf{e}_1$	$\beta\mathbf{e}_2$	$\mathbf{e}_1$	$\mathbf{e}_2$	$\beta\mathbf{e}_1$
$\mathbf{e}_2$	$\mathbf{e}_2$	$\alpha\mathbf{e}_1$	$\alpha\mathbf{e}_2$	$\mathbf{e}_1$
$\mathbf{e}_3$	$\beta\mathbf{e}_0$	$\mathbf{e}_3$	$\mathbf{e}_0$	$\beta\mathbf{e}_3$

The global unite can be computed using the following formula:

$$E = \left(\frac{1}{1-\alpha\beta}, \frac{1}{1-\alpha\beta}, \frac{\beta}{\alpha\beta-1}, \frac{\alpha}{\alpha\beta-1} \right). \quad (2)$$

All vectors $V = (v_0, v_1, v_2, v_3)$ such that $v_0v_1 \neq v_2v_3$ are invertible and compose finite group of the order

$$\Omega = p(p-1)(p^2-1). \quad (3)$$

Number of the non-invertible vectors $N = (n_0, n_1, n_2, n_3)$, where $n_0n_1 = n_2n_3$, is equal to $p^3 + p^2 - p$. A local bi-side unite E' corresponds to each vector N that is not a zero-divisor. The value E' can be computed from the following formula

$$E' = \left(x; \quad \frac{n_2}{n_0\beta + n_2} - \frac{n_0 + n_2\alpha}{n_0\beta + n_2} \cdot \frac{c}{n_0} x; \quad \frac{n_2}{n_0} x; \quad \frac{n_0}{a\beta + n_2} - \frac{n_0 + n_2\alpha}{n_0\beta + n_2} x \right), \quad (4)$$

where $x = n_0(n_2\alpha + n_2 + n_0 + n_3\beta)^{-1}$.

Four-dimensional FNAA elements of which are locally reversible is defined by the BVMT shown as Table 2. In this case the FNAA contains no global unit, however for every vector $V = (v_0, v_1, v_2, v_3)$ such that $v_0v_2 = v_1v_3$ there exists local bi-side unit that can be computed as follows

$$E' = \left(k, \frac{v_0}{\lambda(v_0 + v_3)} - \frac{\mu}{\lambda} k, \frac{v_1}{\mu v_0 + \lambda v_1} - \frac{v_0}{\lambda(v_0 + v_3)} + \frac{\mu}{\lambda} k, \frac{v_0}{\mu v_0 + \lambda v_1} - k \right), \quad (5)$$

where $k = a^2(a+d)^{-1}(\mu a + \lambda b)^{-1}$.

Table 2.

Defining a 4-dimensional FNAA with local reversibility

◊	$\mathbf{e}_0$	$\mathbf{e}_1$	$\mathbf{e}_2$	$\mathbf{e}_3$
$\mathbf{e}_0$	$\mu\mathbf{e}_0$	$\mu\mathbf{e}_1$	$\mu\mathbf{e}_1$	$\mu\mathbf{e}_0$
$\mathbf{e}_1$	$\lambda\mathbf{e}_0$	$\lambda\mathbf{e}_1$	$\lambda\mathbf{e}_1$	$\lambda\mathbf{e}_0$
$\mathbf{e}_2$	$\lambda\mathbf{e}_3$	$\lambda\mathbf{e}_2$	$\lambda\mathbf{e}_2$	$\lambda\mathbf{e}_3$
$\mathbf{e}_3$	$\mu\mathbf{e}_3$	$\mu\mathbf{e}_2$	$\mu\mathbf{e}_2$	$\mu\mathbf{e}_3$

To construct FNAAs of other dimensions one can use some unified BVMTs using which one can define FNAAs of an arbitrary dimension $m > 1$. The unified BVMT is described as matrix containing elements $\mathbf{e}_{ij} = \mathbf{e}_i \circ \mathbf{e}_j$ defined by the following formula:

$$\mathbf{e}_{ij} = \alpha_i \mathbf{e}_j, \quad (6)$$

where $i, j = 0, 1, \ldots, m-1$; $\{\alpha_i\}$ is the set of m different structural coefficients. Properties of the FNAAs defined by formula (6) can be described by some general formulas that hold for an arbitrary value of the dimension m. Each of these algebras contains a subset of its elements representing some set of global right-side units, however only one local right-side unit correspond to an arbitrary fixed m-dimensional vector, except vectors that are square roots of zero vector (0, 0, …, 0). The case $m = 2$ was earlier investigated in [8].

While using some FNAA with global unit the public key agreement scheme uses the following formula for computing the public key: $Y = Q^s \circ G^x \circ Q^{-s}$, where Q and G are invertible elements of the FNAA, which satisfy condition $Q \circ G \neq G \circ Q$ and the pair of integers (s, x) is a private key. Finding the values s and x from the formula for public key is known as hidden logarithm problem (HLP). When using the FNAAs without the global unit one should propose another form for HLP. We propose the following formula for defining the HLP in FNAAs that contain only locally invertible elements:

$$Y = N^s \circ V_E^x \circ N^{\omega - s}, \tag{6}$$

where N and V_E are vectors having large prime local orders ω and τ respectively, such that $N^\omega = E'$ and $N \circ V_E \neq V_E \circ N$.

In the case of sufficiently large dimensions, for example, $m = 6$, 8 and 10 it interesting to define the HLP in the following form

$$Y = N_1^{s_1} N_2^{s_2} \circ V_E^x \circ N_1^{-s_1} N_2^{-s_2}, \tag{7}$$

where the vectors N_1 and N_2 have the same local order ω and satisfy condition $N_1 \circ N_2 = N_2 \circ N_1$. In the case of using the formula (7) one should develop a method for finding the required vectors N_1 and N_2. Besides, respective FNAAs of sufficiently large dimension are to be constructed.

Список литературы

1. Yan S. Y. Quantum Attacks on Public-Key Cryptosystems . – Springer. 2014. – 207 p.
2. Smolin J. A., Smith G., Vargo A. Oversimplifying quantum factoring // Nature. 2013. Vol. 499. No. 7457. P. 163–165.
3. Proceedings of the 7th International Workshop on Post-Quantum Cryptography, PQCrypto 2016. Fukuoka, Japan, February 24-26, 2016 // Lecture Notes in Computer Science (LNCS) series. Springer, 2016. Vol. 9606. - 270 p.
4. Moldovyan D.N. Non-Commutative Finite Groups as Primitive of Public-Key

Cryptoschemes // Quasigroups and Related Systems. 2010. Vol. 18. P. 165−176.

5. Moldovyan D.N., Moldovyan N.A. Cryptoschemes over hidden conjugacy search problem and attacks using homomorphisms // Quasigroups and Related Systems. 2010. Vol. 18. P. 177-186.
6. Moldovyan D.N., Moldovyan N.A. A New Hard Problem over Non-Commutative Finite Groups for Cryptographic Protocols // Springer Verlag LNCS. 2010. Vol. 6258. P. 183−194.
7. Kuzmin A.S., Markov V. T., Mikhalev A. A., Mikhalev A. V., Nechaev A. A. Cryptographic Algorithms on Groups and Algebras // Journal of Mathematical Sciences. 2017. Vol. 223. No. 5. P. 629−641.
8. Moldovyan A.A., Moldovyan N.A., Shcherbacov. V.A., Non-commutative finite associative algebras of 2-dimension vectors // Computer Science Journal of Moldova. 2017. V. 25. No. 3(75). P. 344-356.

ОБРАБОТКА И АНАЛИЗ ИЗОБРАЖЕНИЙ В МЕДИЦИНСКИХ СИСЕМАХ ПОДДЕРЖКИ ПРИНЯТИЯ РЕШЕНИЙ

Обухова Наталия Александровна

доктор технических наук, профессор кафедры Телевидения и видеотехники Санкт-Петербургского государственного электротехнического университета «ЛЭТИ» им. В. И. Ульянова (Ленина), Санкт-Петербург

E-mail: natalia172419@yandex.ru

Мотыко Александр Александрович

кандидат технических наук, доцент кафедры Телевидения и видеотехники Санкт-Петербургского государственного электротехнического университета «ЛЭТИ» им. В. И. Ульянова (Ленина), Санкт-Петербург

E-mail: motyko.alexandr@yandex.ru

IMAGE ANALYSIS AND PROCESSING IN CLINICAL DECISION SUPPORT SYSTEMS

Obukhova Nataliia

doctor of Science, professor at Television and video equipment department of Saint Petersburg Electrotechnical University "LETI", Saint-Petersburg

E-mail: natalia172419@yandex.ru

Motyko Alexander

PhD, assistant professor at Television and video equipment department of Saint Petersburg Electrotechnical University " LETI", Saint-Petersburg

E-mail: motyko.alexandr@yandex.ru

АННОТАЦИЯ

Статья посвящена вопросам обработки и автоматического анализа медицинских видеоданных для систем поддержки принятия решений.

Предложены подходы и алгоритмы, учитывающие специфику медицинских изображений, приведены их характеристики.

ABSTRACT

The paper is devoted to the processing and automatic analysis of medical video data for clinical decision support systems. Approaches and algorithms that take into account the specificity of medical images are offered, their characteristics are given.

Ключевые слова: системы поддержки принятия решений; цифровая обработка медицинских изображений; анализ данных; машинное обучение.

Keywords: CDSS; digital image processing; machine learning; data mining.

CDSS is the modern trend in medical video systems development. Systems of this type realize the integration of automatic image analysis results with the results obtained by the physician, and also use the information of system database.

CDSS development tasks can be divided in two groups. The solution of the tasks from the first group should allow to realize the automatic analysis of image signals with the purpose of differential diagnostics (multi-class analysis). Solving the problems of the second group should ensure the high quality of the images being formed and, as a consequence, the high efficiency of their visual analysis by the physician.

The feature of medical images automatic analysis in CDSS is the need to implement differential diagnostics with the degree of pathology corresponding, which is based on multi-class analysis in conditions of fuzzy borders between classes and high variability of the original data. This determines next principles of image analysis approach. First, the decision rule must be based on the methods which are typical for artificial intelligence systems, such as fuzzy sets theory and fuzzy logic, data mining methods, machine learning and pattern recognition methods. Second, the vector of features for classification must include features with different properties and origins.

This approach was realized by our team in the multispectral TV system for cervix oncological changes diagnosis. The multispectral TV system consists of illuminator, multi-spectral image recorder unit, software and computer. It gives possibility to get images in white light and fluorescent images. The system realizes differential diagnostics of the following changes in cervical tissues as Norm, CNI, CIN I, CIN II, CIN III (cervical intraepithelial neoplasia). So through the implementation of this system the main methods of multispectral images automatic processing and analysis for the differential diagnostics realization will be described in the first part of our report.

The visual analysis of physician is another important part in CDSS. This demands to ensure high quality of the images for physician and, as a consequence, high efficiency of their visual analysis. It demands to develop new methods to improve the quality of medical images and methods for the synthesis of medical images with new properties. These tasks were realized in endoscopic system, described in the second part of paper.

1. *Automated Image Analysis in Multispectral System for Cervical Cancer Diagnostic*

1.1. Image Preprocessing

The effectiveness of image analysis is strong connected with their preprocessing. Standard preprocessing includes procedures to improve the quality of the images such as gamma correction, noise reduction, color balance, etc. Additional for medical image it is necessary to use special preprocessing procedures such as: automatic regions of interest (ROI) segmentation; removing highlights in the images; and in the case of using multi-spectral fluorescent images procedure of their matching.

The images from different modes may have discrepancy in the coordinates, so called shifts. Large shifts between images can noticeably confuse further analysis so the compensation of the shifts between images in different modes must be realized

before tissue classification. The proposed algorithm is based on phase correlation. We compute the cross-power spectrum of analyzing and reference images. The maximum of cross-correlation function determines the spatial displacement between reference image and images which are analyzing. The main advantage of the proposed approach in comparing with the modern algorithms operating in the signal domain is the possibility of matching the images which have significantly different one from another in brightness and color, as well as resistance to noise, occlusion, and similar negative factors of medical images.

On a real medical image, the image of cervix takes only about 70%. The rest part of image may include other tissue, medical instruments, various artefacts. The presence of irrelevant information makes difficult the further data processing and analysis, so it is necessary to select only the image area corresponded to cervix - the region of interest. For automatic region of interest segmentation, we proposed the algorithm based on c-means clustering in chromaticity layer a from Lab color space.

1.2. Image analysis

The main part of cervix multispectral image processing is the classification task. To solve classification task it is necessary to choice features for classification and classifier strategy. There are three groups of pathology signs in the cervix image: brightness and color features, morphological features and texture feature. In our investigation we used for analysis the brightness and color features of image. On the base of our research we decided to use for classification task the next set of features: Cr, Cb (YCrCb system) and b (Lab system) calculated in fluorescent images obtained by excitation with wavelength of 360nm and 390nm.

To select the most appropriate strategy for the classification task we used next set of classifiers: the classification based on Mahalanobis metric (linear discriminate analysis, quadratic discriminate analysis); the classification based on regression model; SVM; PCA with classification by SIMCA (Soft Independent Modeling of Class Analogy); Random decision forest; ADA Boost; Neural networks; the

classification based on fuzzy logic. For classifier training and testing we used approach Leave-one-out cross-validation. The most interesting and the most difficult for design task is the task of classification CNI and CIN. The classification CIN/Norm is rather simple and it is not actual for medicine practice. So at first we calculated the specificity, sensitivity and accuracy on the border CIN/CNI.

Training and validation of classifier was realized on the data base of records, obtained in clinics. Our investigation shows that the best specificity, sensitivity and accuracy are obtained by using Random Decision Forest. The results of RDF classification for the border CNI/CIN are next the sensitivity is 0.85, the specificity 0.78.

Additionally, we estimate specificity and sensitivity on the border Norm/CNI. The results for the border Norm/CIN: the sensitivity is 0.95, the specificity is 0.90.

1.3. The Algorithm of Pathology Map Creation

The main task for pathology map creation is image classification on three classes: Norm, CNI and CIN according the strategy and features chosen above. But besides the classification with the aim of differential diagnostic the pathology map creation demands preliminary classification to select columnar epithelium and artefacts. Because these parts must be eliminated from further analysis. Thus, in our algorithm we use two stages of classification. On the first stage we use 2-class RDF classifier for preliminary classification. We realized the features and the modes selection for this task on the base of Fisher distance and identified that the most effective features are white mode and 360 with the features a and b from the system Lab. On the second stage we use 3-class RDF classifier to separate Norm, CNI and CIN. We use the features Cr, Cb from YCrCb system and b from system Lab for modes 360 and 390. The 3-class RDF classifier means that we have three training samples with examples of all classes. For each one the RDF response is a vector of probabilities of belonging

to each class. We use this probabilities to define the belonging degree to each class and to color the corresponded block on the output map (see Fig. 1).

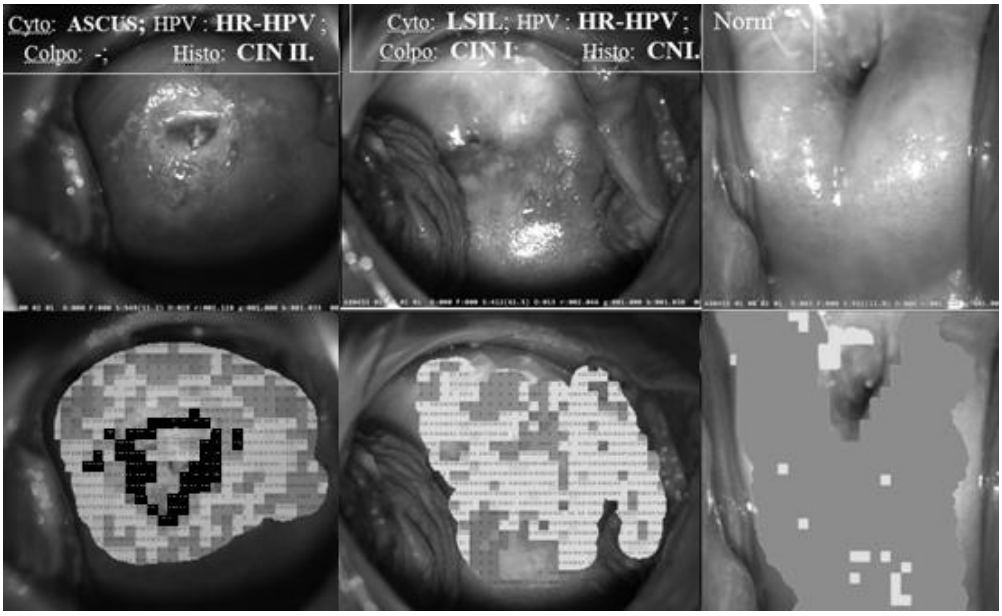

Fig. 1. Examples of pathology map with 3 classes Norm, CNI and CIN

1.4. Results

The experimental investigation and clinical study of proposed algorithm includes two parts. The first part realizes the classifier validation. It was performed on the data base with the leave-one-out strategy. But the main part of the experimental research is the pathology map obtainment and estimation. Analysis of fluorescence images obtained by excitation with wavelength of 360 and 390 nm allows to detect follow states of cervix tissues Norm, CNI, CIN. For the border CIN/CNI we got sensitivity 83% and specificity 72%. These figures correspond to estimates of sensitivity and specificity for colposcopic examination conducted by an experienced physician and exceeds characteristics of inexperienced physician, where the sensitivity and specificity have been reported to range from 87 to 96% and 48 to 85%.

Proposed algorithms give possibility to obtain correct differential pathology map with probability 0.8. Obtained results and classification task characteristics

shown possibility of practical application pathology map based on fluorescents images.

2. Technology of Endoscopy Image Processing for CDSS

The main goal of our endoscopy project is the developing of the new and effective methods of endoscopic image processing providing image enhancement, comfortable visualization, image segmentation and analysis for CDSS.

The important part of the investigation is to develop new method of brightness and contrast enhancement. This task is actual because the endoscopic images suffer from various degradation, and it is necessary to eliminate them before images will be demonstrated to physician. The second part of investigations - method of visualization. Proposed method of panoramic image creation gives possibility to get image with wide viewing angle of organ under supervision, which is comfortable for the analysis and navigation during the physician's inspection and increasing diagnostic values of images.

2.1. Contrast enhancement

In endoscopic images improved contrast is crucial for a correct diagnosis, but the conditions of medical images obtaining are very difficult. In our investigation we used only non-linear techniques. It is connected with main feature of images: there are very dark and very bright areas in the same image. The main methods under investigation were Multi Scale Image Contrast Enhancement [1], Adaptive and Integrated Neighborhood Dependent Approach for Nonlinear Enhancement (AINDANE) [2], Locally Tuned Nonlinear Technique for Color Image Enhancement (LTSNE) [3]. For effectiveness investigation we realized all algorithms. Ehe results of AINDANE and LTSNE are quite similar, but in the most cases the quality of images after LSTNE is slightly higher than after AINDANE enhancement.

The Multi Scale Enhancement is not effective for difficult cases with big dark fields, but for the images with moderate degradations it is useful. The quality of correction is very high and comfortable for visual analysis (Fig.2).

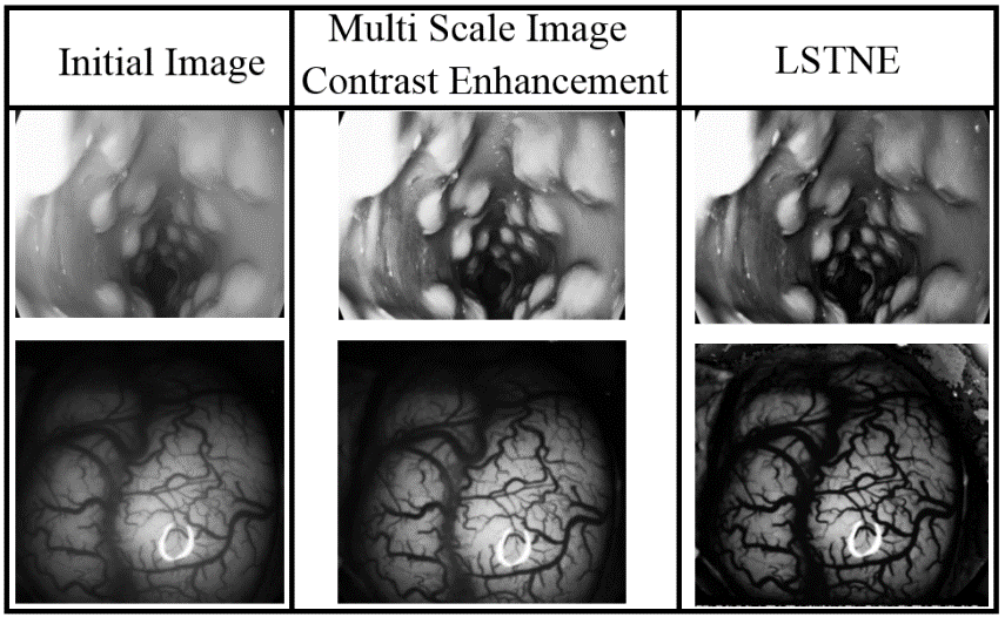

Fig. 2. The illustration of contrast correction algorithms.

The described methods have common drawback. With the increasing of the contrast, the methods significantly emphasize the noise. We propose to consider the local features of the image on the base of the found functional relationship between the correction "strength" p and the normalized variance of brightness in the image fragment. On the stage of contrast enhancement LSTNE applies next transformation function.

$$S(x,y) = 255 \cdot I_{E_n}(x,y)^{E(x,y)},$$

$$E(x,y) = r(x,y)^P = \left(\frac{I_M(x,y)}{I(x,y)}\right)^p.$$

where $S(x,y)$ – pixel brightness after correction, $I_{en}(x,y)$ – normalized brightness, $I(x,y)$ – initial pixel brightness, $I_m\ (x,y)$ – the brightness of a local fragment of an image after filtering, p - parameter for correction "strength". We propose to define p in next way:

$$p = \log\left(\frac{k\sigma^2}{\sigma^2_{min}}\right),$$

where σ – the standard deviation of brightness in a fragment of the image; σ_{min} – the minimum standard deviation of brightness among all fragments of the image; k – parameter of the regression model.

Our investigation showed that the SNR of the image processed by LTSNE and AINDANE falls from 40 dB to 25 dB. The proposed method provides SNR of 35-38 dB on the same fragments of processed images.

2.2. Synthesis of mosaic images for wide angle observation (panoramic images)

One of the main problem of endoscopic images is the narrow field of view. As a result, individual images are often not intuitive for evaluation. Mosaicing offers the opportunity to create an integrated picture of a scene from a video sequence.

The problem of image mosaicing is well studied. In the case of medical images the initial quantity of detail and the quantity of key points is very low. We propose the special procedure for video panorama construction from the images with small quantity of key points. The main features of proposed procedure are:

- the reliability degree for key points matched pairs is introduced. It gives possibility to use the maximum quantity of key points pairs.
- the special modifications of RANSAC method. It supports the using of all found matched points with taking in advance their reliability degree for the source images transformation parameters identification.

The estimation of reliability degree for matched pairs is realized on the base of suppression measure. For each pair of matching key points (pi, pq) the measure of suppression, based on the similarity of the distance between neighboring points on images being stitched ξ is calculated. Then from the set of all matched pairs PQ the set with good matches PQopt with the measure of ξ_i = [0,9...1] and the reliability degree *Rd* = 1 is formed. For each element of the set (PQ – PQopt) the measure of suppression ξ_i = [0...0,9] from the pairs of the set PQopt and the reliability degree Rd = [0...0,9] is calculated via iterative procedure. The introduction of the reliability

degree gives possibility to produce transformation parameters identification with all found matched pairs of key points. This position is ensured by using special proposed modification of RANSAC algorithm - the use of two criteria for selecting the best estimates of the parameters instead one criteria in the base version of RANSAC. The offered method gives possibility to obtain panoramic images in condition of images with low detail (Fig. 3). The average error is less than 0.75 pixels for the video with low quantity of detail.

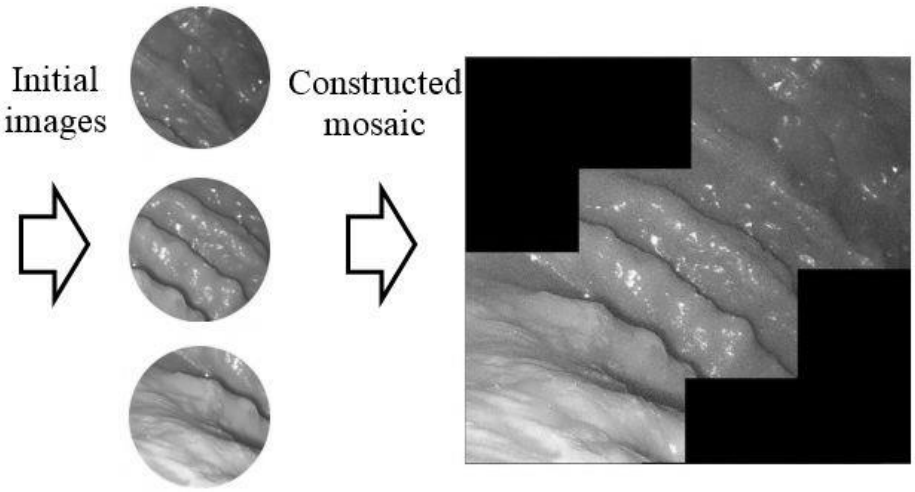

Fig. 3. Mosaic image obtained with proposed method.

2.3. Results

The proposed methods have software realization and were successfully tested on real endoscopic images. The method of endoscopic images processing based on the nonlinear contrast enhancement, allows to save the contrast of the vessels and other small details relative to the background. Proposed method realize contrast enhancement without significant stressing of the noise component, which is one of main disadvantages of modern non-linear enhancement methods, especially in areas of the image with low detail. During our research we created full GPU optimized software pipeline for endoscopic video processing. The CUDA 8.0 was used for GPU programming. The timing of enhancement for FHD is 32 ms.

The method of "mosaic" synthesis creates panoramic image in conditional of low detail in the original video data. The offered method gives possibility to obtain panoramic images in condition of medical images with low detail with average error of stitching less than 0.75 pixels.

Список литературы

1. Vonikakis V., Andreadis I., Multi-Scale Image Contrast Enhancement, 10th Intl. Conf. on Control, Automation, Robotics and Vision, 2008, pp. 856-861.
2. Tao L., Asari K.V., An adaptive and integrated neighborhood dependent approach for nonlinear enhancement of color images, SPIE Journal of Electronic Imaging, Vol. 14, No. 4, 2005, pp. 1.1-1.14.
3. Arigela S., Asari K.V., A Locally Tuned Nonlinear Technique for Color Image Enhancement. WSEAS Trans. Signal Processing 4(8), 2008, pp. 514-519

МОДЕЛИРОВАНИЕ НЕЛИНЕЙНЫХ ЦИФРОВЫХ КОМПЕНСАТОРОВ ПО СООТНОШЕНИЮ ВХОД–ВЫХОД

Соловьева Елена Борисовна

докт. техн. наук, профессор, зав. кафедрой теоретических основ электротехники, Санкт-Петербургский государственный электротехнический университет, Россия, г. Санкт-Петербург

E-mail: selenab@hotbox.ru

INPUT-OUTPUT MODELLING OF NON-LINEAR DIGITAL COMPENSATORS

Elena Borisovna Solovyeva

Doctor of Sciences, Head of Theoretical Electrical Engineering Department, Saint-Petersburg Electrotechnical University "LETI", Russia, Saint-Petersburg

E-mail: selenab@hotbox.ru

АННОТАЦИЯ

Рассматривается моделирование нелинейных устройств, в процессе которого устанавливается однозначное соответствие между множествами входных и выходных сигналов. Описываются математические модели: функциональные полиномы, регрессионные структуры и нейронные сети, применяемые при указанном способе моделирования. Отмечается разнообразие задач, решаемых в рамках моделирования объектов по соотношению вход–выход. На примере подавления нелинейных искажений QAM- и PSK-сигналов в канале связи, описанном структурой Винера, сравниваются полиномиальные и нейронные модели компенсаторов.

ABSTRACT

The modelling of non-linear devices when establishing unique correspondence between the sets of input and output signals is considered. Mathematical models, such as functional polynomials, regression structures and neural networks, used in this modelling approach are described. The variety of the application fields of the

input-output modelling is pointed out. The example of the non-linear distortion suppression in a communication channel described by the Wiener structure under QAM and PSK impacts by using compensators based on polynomial and neural models is represented.

Ключевые слова: математическая модель; полином Вольтерры; нейронная сеть; канал связи; нелинейный компенсатор

Keywords: mathematical model; the Volterra polynomial; neural network; communication channel; non-linear compensator

The functional complexity of analog and digital devices, qualitatively new requirements to characteristics of these devices and a high level of their integration require to improve existing and develop new methods of modelling and synthesis of analog and digital devices.

One of advanced methods of complicated device modelling is based on the mathematical description connecting only the input and output variables of a device [4], [6], [8]. This approach is very useful, for instance, in two situations. Firstly, taking into account of the device component structure the mathematical model of complicated device is described by the equation system with high order. The problem of bad conditionality is emerged on solving this equation system. Secondly, under the lack of sufficient information about the device component structure it is impossible to design the model as the equation system. In mentioned cases to apply the model describing the input-output relationship is the way of the complicated device modelling.

Complicated devices can be generally represented as non-linear dynamic systems, whose input-output relationships are described by non-linear operators [4], [6], [8]. The non-linear operator F_S sets unique connection between the set X of input signals $x(n)$ and the set Y^O of input signals $y^O(n)$, where n is normalized discrete time. Thus, non-linear dynamic system is considered as a “black box” with

the operator F_S such that

$$Y^O = F_S[X]$$

or

$$y^O(n) = F_S[x(n)].$$

For modelling of non-linear dynamic system it is required to approximate the non-linear operator F_S by the non-linear operator F_ε, which reflects the input set X in the output set Y^O with error ε, $\varepsilon > 0$, that is

$$y(n) = F_\varepsilon[x(n)]$$

under condition $\left\| y^O(n) - y(n) \right\| \le \varepsilon$ for all $x(n) \in X$, $y^O(n) \in Y^O$. The non-linear operator F_ε is named the model of non-linear dynamic system.

The parameters of the non-linear operator F_ε result from the solution of the approximation problem

$$\left\| y^O(n) - F_\varepsilon[x(n)] \right\| \to \min_{\mathbf{C}}, \qquad (1)$$

where $\mathbf{C}$ is the vector of the operator F_ε parameters.

The norm in equation (1) can be written as the uniform one

$$\|\bullet\| = \max_{x(n) \in X} \left| y^O(n) - F_\varepsilon[x(n)] \right|$$

or the root-mean-square one

$$\|\bullet\| = \frac{1}{G} \sqrt{\sum_{g=1}^{G} \left(y_g^o(n) - F_\varepsilon\left[x_g(n) \right] \right)^2},$$

where G is the number of signals exciting non-linear system.

The way of solving the approximation problem (1) depends on the form of the non-linear operator F_ε (non-linear model). The universal forms of non-linear model can be divided into two classes.

The first class includes polynomial models [1], [4]–[6], [8], such as

– the Volterra series and the Volterra polynomial,

– the multidimensional polynomial of split signals,

– the NARMAX-model (Non-linear AutoRegressive Moving Average model with eXogenous inputs).

The approximation problem (1) solutions obtained on the basis of polynomial models with linearly incoming parameters are global optimums. As the Volterra series has limited convergence this model is used for simulation of only weakly non-linear systems. The other above mentioned mathematical models can be applied for the approximation of severely non-linear system operators.

The second class of non-linear models is composed of different types of neural networks [1], [3], [5], [7], [9], [13]. These neural networks are characterized as universal approximaters. Let's notice some types of universal approximaters, these are the following [1]:

– multilayer perceptron networks,

– recurrent multilayer perceptron networks (the Elman, Wiener and Hammerstein networks),

– radial bases function networks,

– functional link artificial neural networks (with Chebyshev and Laguerre polynomials),

– spline neural networks,

– wavelet neural networks,

– canonical piecewise-linear networks and recurrent canonical piecewise-linear networks,

– neuro-fuzzy networks (adaptive network based fuzzy inference system, ANFIS).

Neural networks are useful when increasing the polynomial degree gives slowly decreasing the error of the non-linear operator approximation. However, in case of

applying neural networks with nonlinearly incoming parameters to find globally optimal solution of the approximation problem is extremely difficult because of the slow convergence of the calculation algorithm and the emergence of the large number of local optimums.

On the basis of the operator approach, non-linear models can be built for different devices, for instance, compensators, filters, equalizers and so on [1], [2], [9]–[12]. Polynomials and neural networks can be used for the compensator synthesis in electromechanical system sensors, which are described by severely non-linear differential equation.

The example of the non-linear compensator modelling based on the Volterra polynomial and different types of neural networks for the suppression of non-linear distortions in digital communicational channel described by the Wiener model is represented below.

Power amplifiers produce non-linear distortions in the communication channels (CC) [10], [11]. Non-linear distortions generated by a power amplifier draw the wide attention of researchers. The power amplifier is linear in narrow-band and low-power applications. However, the power amplifier operates with width-band signals and as close as possible to saturation to achieve maximum power efficiency and output power. As a result, the power amplifier produces two types of non-linear distortions in the presence of the input signal envelope fluctuation: the dynamic amplitude distortion (AM/AM, amplitude-to-amplitude modulation) and the phase distortion (AM/PM, amplitude-to-phase modulation). The power amplifier nonlinearity leads to signal distortion and appearance of intermodulation components in adjacent channel that cannot be filtered out. The process of out-of-band emission is known as spectral regrowth.

Power amplifiers and bandpass filters are simulated together. Mathematical models are often represented as the Wiener model. The methods of noiseless coding do not enshure the required level of the information transfer reliability. It is expedient

to apply compensators synthesized with the operational approach on the sets of input and output signals in order that the non-linear signal distortions should be cancelled in CC [10], [11].

Let's compensate the non-linear signal distortions in the communication channel described by the Wiener model

$$\dot{x}(n) = d_1\dot{\xi}_1(n) + d_2\dot{\xi}_1^2(n) + d_3\dot{\xi}_1^3(n),$$

where $d_1 = 1$, $d_2 = 0,2$, $d_3 = 0,1$; "$\cdot$" is the sign of complexity; $\dot{x}(n)$ is the output signal of non-linear CC on exciting by the input signal $\dot{\xi}(n)$, which is the complex envelope of modulated signal; $\dot{\xi}_1(n)$ is the output signal of the linear dynamic part of CC with the following transfer function

$$H(z) = (1,0119 - 0,7589\,j) + (-0,3796 + 0,5059\,j)\cdot z^{-1}.$$

Thus, the structure of the Wiener model contains two blocks: linear dynamic part and memoryless nonlinearity. 8PSK-signal and 4QAM-signal are used as input signals $\dot{\xi}(n)$ of CC model.

For suppressing the non-linear CC distortions, non-linear compensators are synthesized on the basis of the following models [1], [3], [5]–[8]:

The Volterra polynomial

$$\dot{y}(n) = \sum_{i_1=0}^{I_1}\sum_{i_2=0}^{I_2}\ldots\sum_{i_{m/2}=0}^{I_{m/2}}\sum_{i_{m/2+1}=0}^{I_{m/2+1}}\ldots$$

$$\ldots\sum_{i_m=0}^{I_m}\dot{C}_{i_1 i_2\ldots i_{\frac{m}{2}} i_{\left(\frac{m}{2}+1\right)}\ldots i_m}\dot{x}^{i_1}(n)\dot{x}^{i_2}(n-1)\ldots$$

$$\ldots\dot{x}^{i_{m/2}}\left(n-\frac{m}{2}\right)\left[\dot{x}^*(n)\right]^{i_{m/2+1}}\ldots\left[\dot{x}_m^*\left(n-\frac{m}{2}\right)\right]^{i_m},$$

where $\dot{y}(n)$ is the output signal of model, $I = I_1 + I_2 + ... + I_{m/2} + I_{(m/2+1)} + ... + I_m$ is the polynomial degree ($I = 3$), $*$ is the sign of complex conjugation, $m/2$ is the memory length ($m = 10$).

The two-layer perceptron

$$\dot{y}(n) = G\left(c_0 + \sum_{i=1}^{I} c_i G\left(\sum_{j=0}^{m} w_{ij} \dot{x}_j(n) \right) \right),$$

where the model input signal is a vector

$$\left[\dot{x}_0(n), \dot{x}_1(n), \dot{x}_2(n), ..., \dot{x}_m(n) \right] =$$

$$= \left[1, \dot{x}(n), \dot{x}(n-1), ..., \dot{x}(n-(m-1)) \right], \quad (2)$$

G is a sigmoid function (hyperbolic tangent), I is the number of neurons ($I = 5$), $(m-1)$ is the memory length ($m = 5$).

The recurrent Hammerstein network

$$\dot{y}(n) = \sum_{r_b=0}^{R_b} b_{r_b} n\dot{e}t^{(2)}(n - r_b) - \sum_{r_a=1}^{R_a} a_{r_a} \dot{y}(n - r_a),$$

where

$$n\dot{e}t^{(2)}(n) = \sum_{k=0}^{I} c_k n\dot{e}t_k^{(1)}(n),$$

$$n\dot{e}t_0^{(1)}(n) = 1,\ n\dot{e}t_k^{(1)}(n) = G\left(\dot{u}_k^{(1)}(n) \right),$$

$$\dot{u}_k^{(1)}(n) = \sum_{l=0}^{m} w_{kl} \dot{x}_l(n),\ k = 1, 2, ..., I,\ \dot{x}_0(n) = 1,$$

the input signal of the compensator model is a vector described by (2), G is a sigmoid function (hyperbolic tangent), I is the number of neurons ($I = 3$), $(m-1)$ is the memory length ($m = 2$), $R_b = 1$, $R_a = 1$.

The root-mean-square error of non-linear compensation is defined by equation

$$\varepsilon = \frac{1}{998}\sqrt{\sum_{n=3}^{1000}\left|\dot{y}(n) - \dot{\xi}(n)\right|^2}$$

The root-mean-square error ε and number Q of the compensator models parameters are represented in tab. 1.

Table 1

Compensation results

Models	**Root-mean-square error and number of models coefficients**	
	ε	Q
Two-layer perceptron	$0{,}6*10^{-3}$	36
Volterra polynomial	$0{,}2*10^{-3}$	286
Recurrent Hammerstein network	$0{,}2*10^{-3}$	16

On the basis of obtained results, it can be observed the following facts:

– non-linear compensators in form of the recurrent neural Hammerstein network and the Volterra polynomial provide the equal accuracy of cancelling non-linear signal distortions for the communication channel designed in the form of the Wiener structure;

– the recurrent neural Hammerstein network surpasses the polynomial model of compensator in the implementation simplicity.

Eventually, using the example of synthesis of the nonlinear signal distortion compensator for a power amplifier, it is shown that among different types of neural networks one can find such a network that provides the high accuracy of signal processing and is simpler than polynomial models.

Список литературы

1. Analysis of mathematical models of continuous and discrete nonlinear systems / U. A. Bichkov, U. M. Inshakov, E. B. Solovyeva, S. A. Scherbakov. – СПб.: Изд-во СПбГЭТУ «ЛЭТИ», 2017.

2. Bianchini M., Maggini M., Jain L. C. Handbook on neural information processing. – Berlin: Springer-Verlag Berlin Heidelberg, 2013.

3. Dreyfus G. Neural networks: Methodology and applications. – Berlin: Springer-Verlag Berlin Heidelberg, 2005.

4. Giri F., Bai E.-W. Block-oriented Nonlinear System Identification. – Berlin: Springer-Verlag Berlin Heidelberg, 2010.

5. Janczak A. Identification of nonlinear systems using neural networks and polynomial models. A Block-Oriented Approach. – Berlin: Springer-Verlag Berlin Heidelberg, 2005.

6. Mathews V. J., Sicuranza G. L. Polynomial signal processing. – New York: John Wiley & Sons, Inc., 2000.

7. Nelles O. Nonlinear System Identification. From classical approaches to neural networks and fuzzy models. – Berlin: Springer-Verlag Berlin Heidelberg, 2001.

8. Ogunfunmi T. Adaptive Nonlinear System Identification. The Volterra and Wiener Model Approaches. – Berlin: Springer-Verlag Berlin Heidelberg, 2007.

9. Patan K. Artificial neural networks for the modelling and fault diagnosis of technical processes. – Berlin: Springer-Verlag Berlin Heidelberg, 2008.

10. RF power amplifier behavioral modelling / D. Schreurs, M. O'Droma, A. A. Goacher, M. Gadringer. – New York: Cambridge university press, 2009.

11. Solovyeva E. B. Dynamic deviation Volterra predistorter designed for linearizing power amplifiers // Radioelectronics and Communications Systems. – 2011. – Vol. 54, № 10. – P. 546-553.

12. Speech, audio, image and biomedical signal processing using neural

networks / Ed.: B. Prasad, S. R. Mahadeva Prasanna. – Berlin: Springer-Verlag Berlin Heidelberg, 2008.

13. Tang H., Tan K. C., Yi Z. Neural networks: Computational models and applications. – Berlin: Springer-Verlag Berlin Heidelberg, 2007.

МЕТОДЫ ПОДАВЛЕНИЯ НЕЛИНЕЙНЫХ КОЛЕБАНИЙ, ВЫЗВАННЫХ РАСКАЧКОЙ САМОЛЕТА ЛЕТЧИКОМ

Зайцева Юлия Сергеевна

Инженер кафедры «Управление сложными системами»,

Университет ИТМО, г. Санкт-Петербург

E-mail: juliazaytsev@gmail.com

THE METHODS OF PREVENTION NONLINEAR PILOT INDUCED OSCILLATION

Zaitceva Iuliia

engineer of Control of Complex Systems Department, ITMO University,

St.Petersburg

АННОТАЦИЯ

Доклад посвящен явлению раскачки самолета летчиком (РСЛ). Приведены модель летчика как элемента контура управления летательного аппарата (ЛА) и моделирование процесса РСЛ. Предотвращение РСЛ представлено с помощью метода последовательной фазовой компенсации в контуре управления ЛА. Приведены численные исследования системы подавления РСЛ с нелинейной коррекцией. Целью доклада является феномен РСЛ. Это явление представляет собой быстро развивающиеся колебания с нарастающей амплитудой по угловым скоростям, перегрузкам и углам, возникающие, главным образом, при стремлении летчика управлять самолетом с высокой точностью. Появление РСЛ тесно связано с наличием нелинейных элементов в контуре управления, прежде всего – с ограничением на скорость отклонения управляющих органов. В докладе показано применение метода последовательной нелинейной коррекции. Разработан алгоритм

последовательной фазовой компенсации в контуре управления ЛА. В результате исследования разработанный метод позволяет предотвратить возникающие колебания ЛА. Доклад проиллюстрирован результатами компьютерного моделирования ситуаций предотвращения РСЛ.

ABSTRACT

The goal of this paper is propose the method of prevention nonlinear oscillation induced by pilot (PIO) appeared in man-machine closed-loop dynamical systems. The prevention of PIO are presented using the series phase-shift compensation method. Computational investigation of prevention PIO using nonlinear correction is reported. The PIO are defined as rapidly developing fluctuations with increasing amplitude of angle rates, angles and g load, generated due to pilot efforts to control the aircraft with a high precision. Advent of PIO is correlated to nonlinear elements in control-loop before everything else like rate constraint of controlled component. The algorithm of series phase-shift compensation in control-loop of aircraft is developed. As a result the developed method is allow to prevent the arising oscillation of unstable aircraft. The report is illustrated by the results of computer simulation of the situation of occurrence and suppression of PIO.

Introduction

The development of new technologies in aviation on the one hand simplifies and automates the work of pilots and on the other hand - introduce new errors and unforeseen disruptions in the operation of flight control systems (FCS). In aviation problems of abnormal interaction were often associated with the introduction of new technologies, functionality or complications. The fly-by-wire technology (FBW) is one of the examples of technologies that have shifted from military aircraft to civilian ones. FBW technology provides opportunities for the emergence of new approaches to solving all types of problems of stability and control of an aircraft. However, the

flexibility inherent in this technology has the potential to create unwanted new side effects and unforeseen problems. In an airplane equipped with an FCS with FBW, the information is transmitted from the cab to the controls in a completely electric way. The cockpit control device can't give the pilot information that the speed limit or the position of the controls of the aircraft has come. As a result, there may be a discrepancy between the pilot's expectations and the actual response of the aircraft. Complexity inherent in developed, excessive FCS, complicates the developers foreseeing all possible interactions between FCS and the pilot. All this led to numerous studies and methods to prevent situations caused by the abnormal interaction of the pilot with the aircraft.

Model of the aircraft-pilot system

In [1, 2] the following linearized aircraft model is given:

$$\dot{x}\,(t) = Ax(t) + B\delta(t), \tag{1.1}$$

where $x = [\alpha, \beta, p, q, r]^T - x_{lin}$, $\delta = [\delta_c, \delta_{re}, \delta_{1e}, \delta_r]^T$, $u = [u_c, u_{re}, u_{1e}, u_r]^T - u_{lin}$, $\alpha, \beta, p, q, r -$ angle of attack, angle of lateral slip, angular velocity of roll, angular velocity in pitch and yaw, respectively. δ and u – are the real and given deviation of the control surface. Suppose that the steering wheel drive is described by second-order equations:

$$\begin{aligned} \dot{\delta}(t) &= \begin{cases} 0, & if\ \left((\delta \geq \bar{\delta}^+)\&(v \cdot \delta > 0)\,\middle|\,(\delta \leq \bar{\delta}^-)\&(v \cdot \delta < 0)\right), \\ v & - \ another\ case \end{cases} \\ \dot{v}(t) &= sat_{\bar{v}}\big(w(t)\big), \\ w(t) &= K_1\big(\delta^*(t) - \delta(t)\big) - K_2 v(t), \end{aligned} \tag{1.2}$$

where $\bar{\delta}^+, \bar{\delta}^- -$ the upper and lower limits of the rudder deflection, $sat_{\bar{v}} -$ the function saturation, $\bar{v} -$ limit of the speed of the control, the coefficients $K_1, K_2 -$ set the value of the characteristic frequency ω_a and the decay rate ξ_a of the linear drive model: $\omega_a = \sqrt{K_1}$, $\xi_a = \frac{K_2}{2\sqrt{K_1}}$. The pilot's task is to track the given pitch angle $\vartheta^*(t)$, using the control lever. The pilot commands are fed to the servo drive,

combined with the angular velocity gyro sensor signal, which is used to provide static stability in the pitch velocity loop. This can be written in the following expression for the control signal directed to the elevator:

$$u_{в}(t) = u_{pilot}(t) - K_q q(t), \quad (1.3)$$

where u_{pilot} – control signal generated by the pilot, K_q – coefficient of damping. Consider a system consisting of a linear drive model and aircraft model. The transfer function (TF) of these series-connected elements has the form:

$$W_{act}(s) = \frac{1.65s+0.91}{(T^2s^2+2\xi T+1)(s^2+s-2.28)} \quad (1.4)$$

The aircraft model is inherently unstable. Thus, it is decided to introduce a damping coefficient K_q into the feedback channel. Using the root hodograph method, we choose $K_q = 4.7$, stability index $\eta = 0.24$, oscillability index $\mu = 1.97$ following [3]. The stability margin of the open-loop system at $K_q = 4.7$ in amplitude is 5.5 dB, in phase 62.6 deg. Following [4], we use the pilot model in the form of a static coefficient together with a pitch deviation error: $u_{в}(t) = K_{pilot}(\vartheta^*(t) - \vartheta(t))$ and (1.3) states that:

$$u_{в}(t) = K_{pilot}(\vartheta^*(t) - \vartheta(t)) - K_q q(t) \quad (1.5)$$

Extension of the model (1.1), (1.3) – (1.5) by the kinematic equation $\dot{\vartheta}(t) = q(t)$, which describes the relationship between the angular velocity along the pitch and the horizon angle. The optimal transient for system (1.4) gives $K_{pilot} = 4.5$. The resulting stability margin of close-loop system in amplitude is 14 dB, in phase – 66.5 deg.

Development of an algorithm for series phase compensation in aircraft control-loop

Series nonlinear correction

Correction devices are used to approximate the characteristics of the

automatic control system (ACS), consisting of the necessary elements, to the desired characteristics. The methods of synthesizing CS are usually reduced to determining the type and parameters of corrective device [3, 5]. With the help of a link with a specially selected nonlinear static characteristic, the static characteristic of the entire ACS as a whole can be aligned or deformed. The introduction of the nonlinear corrective device (NCD) into a control system with nonlinearities such as saturation, friction, dead zone reduces the speed of the transient process, suppresses self-oscillations [6]. Including the NCD in the ACS, they achieve an increase in the phase response in the cutoff frequency rang, leaving the amplitude characteristic unchanged, thereby reducing the noise acting on the system. Independence of the amplitude characteristic from the frequency change greatly simplifies the design process of the automatic control system. Following the method of [7, 8], in order to prevent the PIO, we introduce a serial NCD of the form:

$$W(s) = \frac{T_1}{T_2} \cdot \frac{T_2 s+1}{T_1 s+1}, \quad (1.7)$$

where $0 < T_1 < T_2 -$ time constant, denoted by $\nu = T_1/T_2$. Phase shift introduced by the filter (1.7): $\varphi(\omega) = arctan\omega T_2 - arctan\omega T_1 > 0$. As a result of harmonic linearization of this nonlinear element with a linear filter (1.6), the following expressions are obtained for its logarithmic amplitude and phase characteristics (LAC, LPC) as a function of ν:

$$H(A,\omega) = \sqrt{a(A,\omega)^2 + b(A,\omega)^2}, \quad (1.8)$$

$$\varphi(A,\omega) = arctan\frac{b(A,\omega)}{a(A,\omega)}$$

Harmonic linearization coefficients for (1.6):

$$a = \frac{k}{\pi}(\pi - 2\varphi + sin2\varphi), b = \frac{k}{\pi}(1 - cos2\varphi). \quad (1.9)$$

The calculations gives the phase characteristic of the NCS has 70 deg with ν=0.01. At the same time, the attenuation of the amplitude hardly reaches -

4 dB, which does not affect the operation of the system. This shows a positive phase shift between $u(t) = sin\Omega t$ and $y(t)$, which demonstrates the phase-leading property of the filter. Modeling parameters: $\nu = 0.1, A = 1, \Omega = 2$ rad/s.

Investigate of uncorrected system

The demonstration of the properties of the nonlinear phase-pre-filter (1.8) is shown on the model of an aircraft. We will simulate a system with a drive with constrains at $K_{pilot} = 4.5$. The simulation results are shown in Figure 1.1. It can be seen from the figure that the quality of the processes is unsatisfactory.

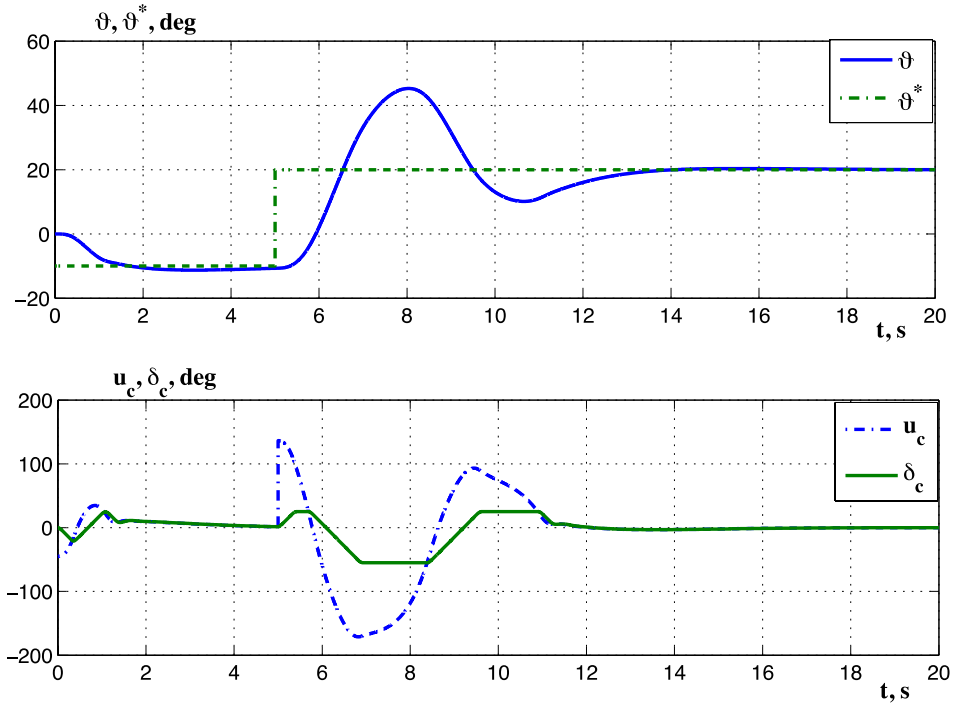

Fig. 1.1 — A system with drive limitations

Investigation of the corrected system

We introduce the NKD into the direct control channel and consider the behavior of such a system. The simulation results in Figures 1.2 show that the introduction of nonlinear correction allow to increase the level of the input signal, as well the pilot gain. The higher the signal level, the more relaxed and ≪ *smoother* ≫ the pilot has to act.

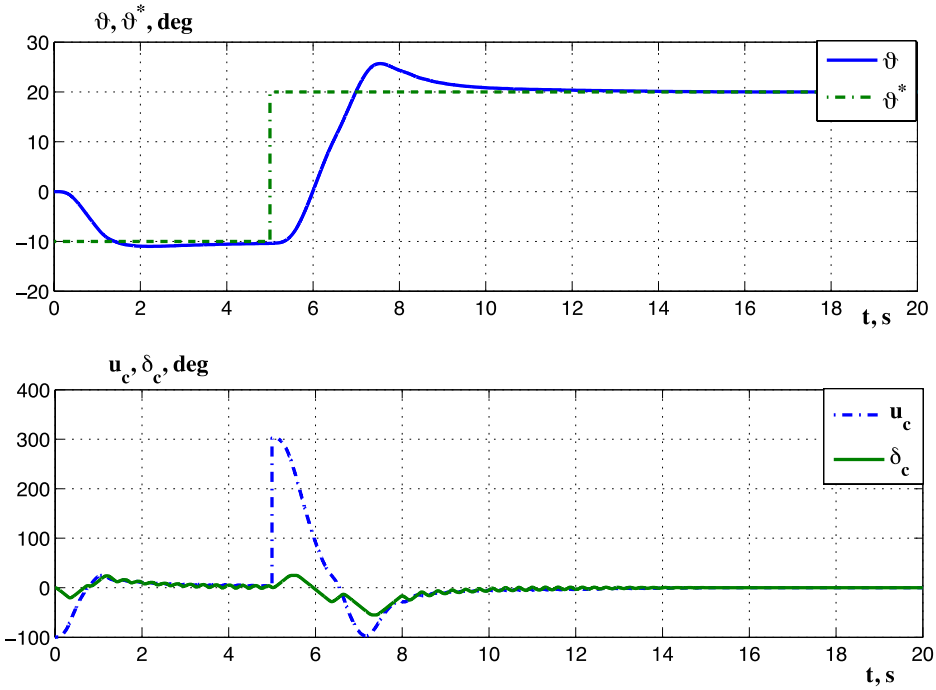

Fig. 1.2 — Adjusted system with drive limitations $K_{pilot} = 10$

Investigation of the system with delay

Let us introduce the delay element into the straight line. Let us take the time delay $\tau = 0.2$ s. The results of the simulation are shown in Figure 1.3, and show the acceptability of process quality.

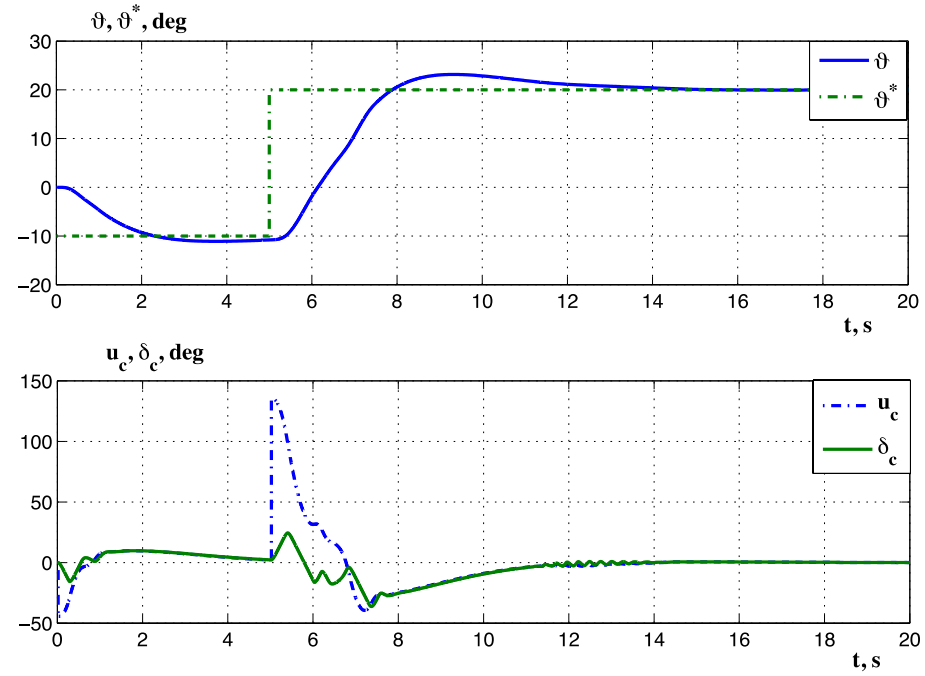

Fig. 1.3 — Adjusted system with nonlinear drive $K_{pilot} = 10$

Conclusion

The results show that the proposed method of nonlinear phase correction in the control loop of a manned aircraft in an autonomous system allows to increase the allowable pilot gain, and therefore make it possible for the pilot to respond more vigorously to a signal mismatch on the one hand, and to prevent PIO, safety on the other. Thus, in this work, a nonlinear correction device was synthesized that allows the pilot to expand the boundaries of his interaction with the flight control system through the control body. We can add that for such relatively simple systems as in this paper, there are no full-fledged analytical methods based not only on modeling. Achieving stability in a state of equilibrium, we don't get a guarantee of stability in the case of working off the driving force or the appearance of disturbing influences. It should be noted that in the study of nonlinear systems, it is necessary to take into account the different forms and parameters of the input (reference) signals taken from [9, 10]. Therefore the presented results don't give the recommended value for the pilot gain. For practical use, it requires deep research, intensive modeling, including real flight tests.

This work was supported by the Government of the Russian Federation, Grant 08-08.

Список литературы

1. Harkegard S. O., Glad T. Resolving actuator redundancy – optimal control vs. control allocation // Automatica. 2005. Vol. 41. P. 137–144.
2. Yildiz Y., Kolmanovsky I., Acosta D. A control allocation system for auto- matic detection and compensation of phase shift due to actuator rate limiting // Proc. American Control Conference. 2011.P.444–449.
3. Бесекерский В.А., Попов Е.П. Теория систем автоматического регулирования. М.: Наука, 1975. С. 768 с.

4. Rundqwist L., Stâhl-Gunnarsson K. Phase compensation of rate limiters in unstable aircraft // Proc. Int. Conf. Control Applications (CCA'96). Dearborn, MI, USA: IEEE Press, Piscataway, NJ, 1996. P. 19–24.
5. Юревич Е.И. Теория автоматического управления. Москва: Энергия, 1969. С. 375.
6. Нелинейные корректирующие устройства в системах автоматического управления / Под ред. Попов Е.П. М.: Машиностроение, 1971.
7. Andrievsky B., Kuznetsov N., Kuznetsova O. et al. Nonlinear Phase Shift Compensator for Pilot-Induced Oscillation Prevention // Prepr. 9th IEEE Europ. Modeling Symp. on Mathematical Modeling and Computer Simulation (EMS 2015). Madrid, Spain: 2015. 6 - 8 October. P. 225–231. URL: http://uksim.info/ems2015/start.pdf.
8. Andrievsky B., Kravchuk K., Kuznetsov N. et al. Hidden oscillations in the closed-loop aircraft-pilot system and their prevention // IFAC - PapersOn-Line. 2016. Vol. 49. P. 30–35.
9. van den Berg R., Pogromsky A. Y., Rooda J. E. Uniform Convergency for Marginally Stable Lur'e Systems with Saturation Nonlinearity, with Application in Anti-Windup Systems // Automatica. 2010. to appear.
10. Andrievsky B., Kuznetsov N., Leonov G., Pogromsky A. Convergence Based Anti-windup Design Method and Its Application to Flight Control // Proc.IV Int. Congress on Ultra Modern Telecom. and Control Systems. St.Petersburg, Russia: IEEE, 2012. 3–5. P. 219–225.

Оглавление

3-я Конференция по алгоритмам в Санкт-Петербурге (SPbAW-2018)

(Санкт-Петербург, 28 мая 2018 г.)

Материалы конференции изданы в авторской редакции

Главный редактор – Кирсанов К.А.

Вёрстка – Кирсанов К.К.

Ответственный за выпуск - Алимова Н.К.

Научное издание

Системные требования:
Системные требования: IBM PC с процессором Pentioum 2; ОЗУ 128 Мб; операц. система Windows XP; программа Adobe PDF Reader; CD-ROM дисковод, мышь.

Режим доступа: http://izd-mn.com/PDF/19MNNPK18.pdf, свободный. – Загл. с экрана. - Яз. рус., англ.

ООО «Издательство «Мир науки»

«Publishing company «World of science», LLC

Адрес:

Юридический адрес — 127055, г. Москва, пер. Порядковый, д. 21, офис 401.

Почтовый адрес — 127055, г. Москва, пер. Порядковый, д. 21, офис 401.

http://izd-mn.com